

MULTI-LEVEL MONTE CARLO DROPOUT FOR EFFICIENT UNCERTAINTY QUANTIFICATION

AARON PIM AND TRISTAN PRYER

ABSTRACT. We develop a multilevel Monte Carlo (MLMC) framework for uncertainty quantification with Monte Carlo dropout. Treating dropout masks as a source of epistemic randomness, we define a fidelity hierarchy by the number of stochastic forward passes used to estimate predictive moments. We construct coupled coarse–fine estimators by reusing dropout masks across fidelities, yielding telescoping MLMC estimators for both predictive means and predictive variances that remain unbiased for the corresponding dropout-induced quantities while reducing sampling variance at fixed evaluation budget. We derive explicit bias, variance and effective cost expressions, together with sample-allocation rules across levels. Numerical experiments on forward and inverse PINNs–Uzawa benchmarks confirm the predicted variance rates and demonstrate efficiency gains over single-level MC-dropout at matched cost.

1. INTRODUCTION

In many scientific computing and machine learning applications, neural networks are increasingly used as fast surrogate models for complex simulations [RPK19]. Unlike traditional mechanistic models, these neural surrogates do not by default quantify prediction uncertainty. Their outputs are deterministic. In practice this is problematic: deep networks often interpolate training data well but can make overconfident, erroneous predictions when extrapolating [Gaw+23; HW21]. In applied surrogate pipelines this lack of uncertainty can be a practical barrier to reliable deployment, including settings where the surrogate is used for repeated evaluation and decision making [PP25].

Consequently, there is a pressing need to accompany neural surrogates with uncertainty quantification (UQ). Bayesian deep learning methods address this by modelling a distribution over network outputs. For example, Monte Carlo dropout (MC-dropout) interprets dropout at test time as approximate Bayesian inference, yielding epistemic uncertainty estimates without changing network architecture [GG16]. Similarly, methods like deep ensembles train multiple networks and use the ensemble variance for UQ [LPB17]. In scientific machine learning, Physics-informed Neural Networks (PINNs) incorporate prior knowledge by training on physics constraints, but they too generally lack calibrated uncertainty outputs unless extended to Bayesian formulations. For inverse problems and constrained training setups this can be especially acute, since inference is driven by a combination of data mismatch and modelling assumptions [Cox+24; MPP24]. In such settings one may face both aleatoric uncertainty (inherent noise in data) and epistemic uncertainty (model uncertainty) [KG17]. In this work we focus on reducing the cost of estimating epistemic uncertainty induced by MC-dropout.

A standard approach (as in MC-dropout or ensemble sampling) is to run many stochastic forward passes to estimate predictive statistics. However, the computational cost grows linearly with the number of samples. Reducing estimator variance by increasing the number of samples can be prohibitive in large-scale settings. For example, MC-dropout often uses dozens of passes per input to estimate uncertainty, each pass incurring a full forward evaluation of the network. This renders uncertainty estimation expensive for large or real-time models and it is already a practical bottleneck in surrogate pipelines that require repeated uncertainty evaluation [PP25]. More generally, naive Monte Carlo estimators are often too costly when each sample is expensive [Gil15].

Multilevel Monte Carlo (MLMC) addresses precisely this issue by exploiting a hierarchy of fidelities and a telescoping decomposition [Hei01; Gil08]. Most samples are taken at low-fidelity (cheap) levels and few at high-fidelity (expensive) levels, reducing total cost for a given error [Gil08; Gil15]. In stochastic simulation (e.g. SDEs and PDEs) MLMC has proven very effective [Cli+11]. Recent work has begun to bring MLMC ideas into machine learning; for instance, [FS21] applies MLMC to variational inference in Bayesian models

and [Ger+21] proposes multilevel training strategies for deep networks. More closely related to our setting, [Bla+23] develops an unbiased MLMC scheme to speed up dropout training of classifiers. However, to our knowledge MLMC has not been explored for inference-time uncertainty quantification in neural surrogates.

The goal of this work is to bridge practical dropout-based uncertainty estimation with variance-reduction tools from multilevel Monte Carlo (MLMC). We formulate an MLMC framework in which Monte Carlo dropout provides the randomness, a single forward evaluation with dropout is treated as a randomised model evaluation and predictive statistics are estimated by sampling over dropout masks. Our primary notion of fidelity is the number T of stochastic forward passes used inside the predictive estimators. Higher fidelity corresponds to more dropout masks and hence higher computational cost. Building on this hierarchy, we construct multilevel estimators by coupling coarse and fine evaluations through shared dropout masks, so that level corrections have reduced variance. This yields multilevel estimators for both dropout-induced predictive expectations and dropout-induced predictive variances, while retaining unbiasedness for these dropout-induced targets. Other notions of fidelity, such as varying dropout probability or using a hierarchy of network resolutions, can also be viewed through a multilevel lens, but they require additional modelling choices and are not essential for the core development presented here.

We provide a theoretical analysis of the resulting estimators. We derive explicit bias, variance and cost expressions, identify the quantities that control the variance of level corrections and use these to formulate sample allocation strategies across levels under a coupled cost model with mask reuse. The resulting allocations recover the classical MLMC structure $M_\ell \propto \sqrt{V_\ell/C_\ell}$, with problem-specific expressions for the level variances V_ℓ induced by the dropout coupling. We also discuss practical ladder design and stopping criteria based on empirical level-variance estimates.

We demonstrate the approach on benchmark problems drawn from scientific machine learning. First, we consider a forward PINNs–Uzawa problem for a boundary-layer ODE with a known closed-form solution and study the behaviour of single-fidelity and multilevel dropout estimators, including empirical verification of the predicted sampling-variance rates and a fixed-cost allocation test. Second, we consider an inverse PDE-constrained optimisation benchmark with a stochastic target generated by a scalar noise variable, for which the ground-truth target moments are available in closed form. In both settings we report how the estimator variances depend on the fidelity ladder and on the sample allocation, and we compare empirical best allocations with the continuous allocations predicted by the theory.

Research on uncertainty for neural surrogates spans several strands that intersect in this work. Dropout, originally introduced for regularisation [Sri+14], can be kept active at test time and interpreted as approximate Bayesian inference, providing a practical route to epistemic uncertainty without changing architecture or training [GG16]. A related theme is the distinction between aleatoric uncertainty (stemming from data noise) and epistemic uncertainty (stemming from model uncertainty), which is now standard in uncertainty-aware deep learning [KG17]. Complementary strategies include Bayesian neural networks and deep ensembles, where independent predictors provide variance-based estimates that are often strong in practice [LPB17]. In scientific surrogate pipelines, MC-dropout has also been used directly as a practical UQ tool when repeated uncertainty evaluation is required [PP25].

Multilevel Monte Carlo provides a cost–accuracy tradeoff that is well suited to expensive stochastic evaluation. Foundational results establish telescoping estimators over coupled fidelity levels and show that, in canonical discretisation settings, complexity improvements such as $O(\varepsilon^{-3})$ to $O(\varepsilon^{-2})$ can be achieved under standard assumptions on bias, variance decay and per-sample cost [Hei01; Gil08; Gil15]. The methodology has been widely validated in stochastic simulation for SDEs and PDEs, including elliptic problems with random coefficients [Cli+11]. In this paper we exploit the same principles at inference time for neural predictors by introducing a hierarchy of estimators for MC-dropout and coupling them across fidelities so that level differences have low variance.

Recent work begins to explore multilevel ideas within machine learning itself. Examples include multilevel variance reduction for stochastic variational inference [FS21], hierarchical training strategies for networks [Ger+21] and unbiased multilevel constructions that accelerate dropout training [Bla+23]. There is also growing interest in multilevel and multi-fidelity approaches for simulation-based inference when multiple simulators are available, demonstrating improved performance at fixed computational budgets with appropriate couplings [Hik+25]. The present contribution is distinct in its focus on inference-time uncertainty

quantification for neural surrogates, where multilevel sampling targets the cost of estimating MC-dropout moments.

Within scientific machine learning, physics-informed neural networks provide a flexible framework for solving forward and inverse problems but generally require dedicated mechanisms for calibrated uncertainty [RPK19]. Bayesian variants and multi-fidelity uncertainty-aware surrogates have been developed to address this [YMK21; MBK21]. In our setting, PINN surrogates benefit from treating MC-dropout estimators as levelled evaluations, allowing dropout-induced epistemic uncertainty to be computed with substantially fewer expensive forward passes.

Overall, this paper synthesises MC-dropout for epistemic uncertainty [GG16], uncertainty-aware surrogate modelling in scientific applications [RPK19; MBK21] and multilevel Monte Carlo for computational efficiency [Gil15; FS21]. The result is a framework that targets the computational cost of uncertainty estimation and demonstrates that multilevel sampling can deliver accurate dropout-based UQ for neural surrogates at reduced budgets.

The rest of the paper is set out as follows. In §2 we define the dropout-induced targets of interest and introduce multilevel Monte Carlo estimators for the predictive mean and variance based on coupled inner fidelities. In §3 we give a practical coupled sampling algorithm, define the coupled cost model under mask reuse and derive optimal sample allocations across levels for a fixed computational budget. In §4 we validate the theoretical predictions on forward and inverse PINNs–Uzawa benchmarks, including empirical variance-rate studies and fixed-cost allocation tests. In §5 we summarise implementation details relevant to reproducibility and computational complexity. We conclude in §6. An appendix collects supporting proofs of the technical lemmata used in the analysis, including covariance identities for overlapping sample-variance estimators and proofs of the allocation formulae.

2. MULTILEVEL ESTIMATORS FOR MC-DROPOUT MOMENTS

In this section we formulate MC-dropout inference as the numerical estimation of moments of a randomised network output. This viewpoint makes the computational bottleneck explicit, uncertainty estimates require many stochastic forward passes. We then develop multilevel Monte Carlo estimators that reduce this cost while targeting the same dropout-induced quantities.

2.1. Dropout-induced random predictor. We begin by fixing a deterministic surrogate model represented by a trained feedforward neural network. Concretely, for an input $x \in \mathbb{R}^{N_{\text{in}}}$ the network produces an output in $\mathbb{R}^{N_{\text{out}}}$ via a composition of affine maps and a nonlinearity. For example, writing $z_0 := x$ and, for $k = 0, \dots, K - 1$,

$$(1) \quad z_{k+1} := \sigma(W_k z_k + b_k), \quad \mathcal{D}(x; \hat{\theta}) := W_K z_K + b_K,$$

where σ is an appropriate activator, $\hat{\theta} := \{(W_k, b_k)\}_{k=0}^K \in \Theta$ denotes the trained weights and biases, held fixed throughout this section. A schematic of this deterministic evaluation is shown in Figure 1.

In MC-dropout, dropout is kept active at evaluation. Each forward pass therefore draws a random collection of dropout masks, which are applied to selected layer activations. For a given $\hat{\theta} \in \Theta$, we collect all such sources of test-time randomness into a random element $\theta \sim \pi_{\hat{\theta}}$, where $\pi_{\hat{\theta}}$ is the associated probability law induced by the chosen dropout rates and parameters $\hat{\theta} \in \Theta$.

In the specific case of MC-dropout, and for fixed learned parameters $\hat{\theta}$, the random element θ may be identified with the collection of Bernoulli masks applied across all dropout layers during a single forward pass. Concretely, for a dropout layer of width N_{width} we draw a mask

$$(2) \quad \mathbf{B} = (B_1, \dots, B_{N_{\text{width}}})^{\top}, \quad B_j \stackrel{\text{iid}}{\sim} \text{Bernoulli}(1 - p_{\text{drop}}),$$

where $p_{\text{drop}} \in (0, 1)$ denotes the dropout probability. A typical dropout layer then acts as

$$(3) \quad z_{k+1} := \mathbf{B}^{(k)} \odot \sigma(W_k z_k + b_k),$$

where \odot denotes componentwise multiplication. (Any standard dropout scaling convention, such as inverted dropout, is absorbed into the definition of $\mathcal{D}(x; \theta)$.)

Collecting the instances of the dropout masks $\{\mathbf{B}^{(k)}\}_{k=0}^{L-1}$ and pairing them with the trained weights $\hat{\theta} \in \Theta$, yields a single realisation of $\theta \sim \pi_{\hat{\theta}}$. Repeated stochastic forward passes correspond to independent draws $\theta_1, \theta_2, \dots \stackrel{\text{iid}}{\sim} \pi_{\hat{\theta}}$ with $\hat{\theta}$ held fixed. For notational simplicity we write the resulting randomised predictor as $\mathcal{D}(x; \theta)$, with the understanding that $\hat{\theta}$ is fixed and θ encodes only test-time randomness. This stochastic evaluation is illustrated in Figure 2.

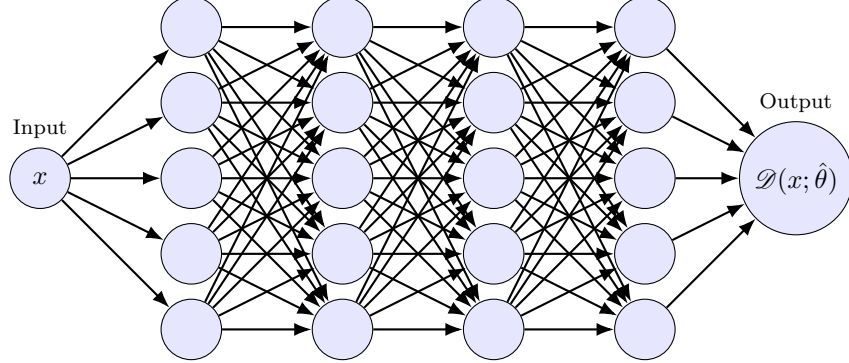


FIGURE 1. Schematic of the surrogate network architecture in its deterministic form. The trained parameters $\hat{\theta}$ are fixed and repeated evaluations produce identical outputs $\mathcal{D}(x; \hat{\theta})$.

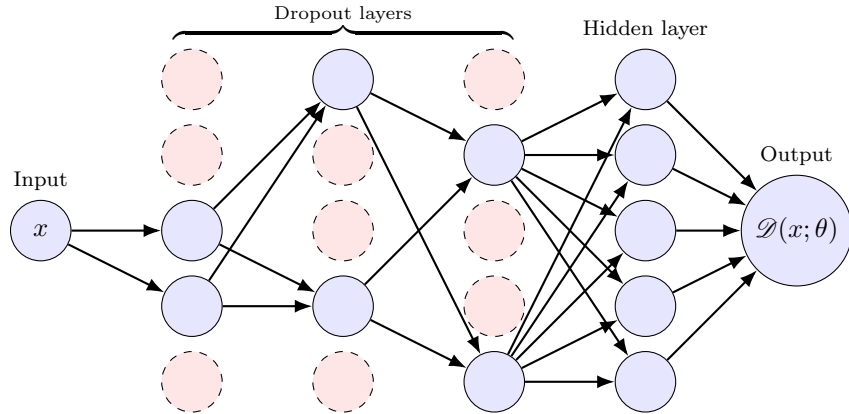


FIGURE 2. The same network evaluated with dropout active. Each forward pass draws dropout masks (encoded in $\theta \sim \pi_{\hat{\theta}}$), yielding a randomised output $\mathcal{D}(x; \theta)$. Repeated evaluations resample θ and can therefore produce different outputs.

Throughout this section we present the moment identities in the scalar-output case $N_{\text{out}} = 1$, so that $\mathcal{D}(x; \theta) \in \mathbb{R}$ and $\mu_2(x)$ denotes the predictive variance. For vector-valued outputs $\mathcal{D}(x; \theta) \in \mathbb{R}^{N_{\text{out}}}$, the same constructions and results apply componentwise by applying the definitions below to each coordinate of $\mathcal{D}(x; \theta)$.

We are interested in the first two central moments of this randomised predictor with respect to the epistemic randomness induced by dropout. We denote these by

$$(4) \quad \mu(x) := \mathbb{E}_{\theta}[\mathcal{D}(x; \theta)], \quad \mu_2(x) := \text{Var}_{\theta}[\mathcal{D}(x; \theta)] = \mathbb{E}_{\theta}[(\mathcal{D}(x; \theta) - \mu(x))^2].$$

We use the notation μ, μ_2 to emphasise that these are moments of the dropout-induced predictive distribution at fixed x . This choice is convenient later when we introduce sample estimators and their sampling variances, where using σ^2 for multiple distinct variances can become ambiguous.

In the analysis of variance estimators we will also require the fourth central moment, which we denote by

$$(5) \quad \mu_4(x) := \mathbb{E}_\theta \left[(\mathcal{D}(x; \theta) - \mu(x))^4 \right].$$

This moment controls the sampling variability of empirical variance estimators and will therefore enter the allocation and complexity results.

The randomness in $\mathcal{D}(x; \theta)$ captures epistemic uncertainty arising from limited data and model uncertainty, and should be distinguished from aleatoric uncertainty, which represents irreducible variability or systematic effects in the data-generating process. The dropout-induced predictive distribution is not the exact Bayesian predictive distribution, since dropout provides only a variational approximation to Bayesian inference [GG16]. A known limitation is that the resulting uncertainty estimates can be miscalibrated, for example due to architecture choice, dropout rate or unmodelled aleatoric noise [Guo+17]. Nonetheless, MC-dropout is computationally lightweight and is widely used as a practical route to epistemic uncertainty estimation [Gal16; KG17].

2.2. Single-fidelity Monte Carlo estimators. To approximate the dropout-induced moments (4) at a fixed input x , a natural approach is Monte Carlo sampling over independent realisations of the test-time randomness. Let $\{\theta_t\}_{t=1}^T$ be i.i.d. draws from $\pi_{\hat{\theta}}$, the law induced by dropout for fixed weights $\hat{\theta}$, written $\theta_t \stackrel{\text{iid}}{\sim} \pi_{\hat{\theta}}$. For notational simplicity, we omit the explicit dependence of the associated probability law $\pi_{\hat{\theta}}$ on the trained weights $\hat{\theta} \in \Theta$, and denote the law by π . We then define the single-fidelity (single- T) estimators of the predictive mean and predictive variance by

$$(6) \quad Y(x; T) := \frac{1}{T} \sum_{t=1}^T \mathcal{D}(x; \theta_t), \quad V(x; T) := \frac{1}{T-1} \sum_{t=1}^T (\mathcal{D}(x; \theta_t) - Y(x; T))^2.$$

Here T is the fidelity parameter, larger T yields lower sampling variability but requires more stochastic forward passes.

2.2.1. Moments of single-fidelity estimators. The estimators $Y(x; T)$ and $V(x; T)$ are random variables, since they depend on the random draws $\{\theta_t\}_{t=1}^T$. Their expectations recover the target moments (4), and their sampling variances quantify the accuracy of a single Monte Carlo estimate at fidelity T .

Lemma 2.3 (Moments of single-fidelity estimators). *If $\theta_t \stackrel{\text{iid}}{\sim} \pi$ and $T \geq 2$, then*

$$(7) \quad \begin{aligned} \mathbb{E}[Y(x; T)] &= \mu(x), & \text{Var}[Y(x; T)] &= \frac{1}{T} \mu_2(x), \\ \mathbb{E}[V(x; T)] &= \mu_2(x), & \text{Var}[V(x; T)] &= \frac{1}{T} \left(\mu_4(x) - \frac{T-3}{T-1} \mu_2^2(x) \right), \end{aligned}$$

where $\mu_4(x)$ is defined in (5).

2.3.2. Outer sampling and empirical estimators. In applications we often wish to quantify not only the estimators $Y(x; T)$ and $V(x; T)$ themselves, but also their sampling variability $\text{Var}[Y(x; T)]$ and $\text{Var}[V(x; T)]$. A direct empirical approach is to draw M independent *replicates* of the estimators (6). That is, for $m = 1, \dots, M$, let $\{\theta_t^{(m)}\}_{t=1}^T$ be i.i.d. draws from π , and define

$$Y^{(m)}(x; T) := \frac{1}{T} \sum_{t=1}^T \mathcal{D}(x; \theta_t^{(m)}), \quad V^{(m)}(x; T) := \frac{1}{T-1} \sum_{t=1}^T (\mathcal{D}(x; \theta_t^{(m)}) - Y^{(m)}(x; T))^2.$$

We then form the empirical estimators

$$(8) \quad \begin{aligned} \bar{Y}(x; M, T) &:= \frac{1}{M} \sum_{m=1}^M Y^{(m)}(x, T), & \mathcal{S}_Y^2(x; M, T) &:= \frac{1}{M-1} \sum_{m=1}^M (Y^{(m)}(x, T) - \bar{Y}(x; M, T))^2, \\ \bar{V}(x; M, T) &:= \frac{1}{M} \sum_{m=1}^M V^{(m)}(x, T), & \mathcal{S}_V^2(x; M, T) &:= \frac{1}{M-1} \sum_{m=1}^M (V^{(m)}(x, T) - \bar{V}(x; M, T))^2. \end{aligned}$$

The single-fidelity construction requires MT evaluations of $\mathcal{D}(x; \theta)$ and therefore has cost scaling linearly in both M and T . Achieving small empirical variances $\mathcal{S}_Y^2(x; M, T)$ and $\mathcal{S}_V^2(x; M, T)$ can therefore become

computationally expensive. This motivates the multilevel constructions introduced in the next subsection, which aim to reduce cost for a prescribed accuracy by combining several fidelities.

2.4. Multilevel estimator for the predictive mean. We now construct a multilevel Monte Carlo (MLMC) estimator for the dropout-induced predictive mean $\mu(x)$. The key idea is to combine estimators of increasing fidelities $T_0 < \dots < T_L$, using many cheap low-fidelity samples and few expensive high-fidelity samples, while coupling neighbouring fidelities to reduce the variance of level differences.

Remark 2.5 (Estimator hierarchy rather than discretisation hierarchy). *In contrast to classical MLMC for biased discretisations, the estimators $Y(x, T_\ell)$ defined in (6) are unbiased for $\mu(x)$ for every ℓ . The fidelity parameter T_ℓ controls sampling variance and cost, not modelling bias. The multilevel construction therefore acts as a structured control-variate scheme built from coupled estimators of the same target moment.*

2.5.1. *Coupling across fidelities.* Fix a strictly increasing sequence of fidelities

$$(9) \quad 1 \leq T_0 < T_1 < \dots < T_L,$$

and let $\mathbf{T} := (T_0, \dots, T_L)$ and $\mathbf{M} := (M_0, \dots, M_L)$ denote the fidelity ladder and the corresponding numbers of samples (per level). The MLMC construction couples *neighbouring* fidelities within each level difference: for a fixed level $\ell \geq 1$ and outer index $m \in [1, M_\ell]$, we form a coupled pair $(Y^{(m)}(x, T_{\ell-1}), Y^{(m)}(x, T_\ell))$ by reusing the first $T_{\ell-1}$ dropout realisations inside the T_ℓ -sample mean, and generating only $T_\ell - T_{\ell-1}$ additional draws. Dropout realisations are sampled independently across outer replications m , so that for any fixed ℓ the estimators $Y^{(m_1)}(x; T_\ell)$ and $Y^{(m_2)}(x; T_\ell)$ are independent whenever $m_1 \neq m_2$, while for a given m the samples used at fidelity $T_{\ell-1}$ are reused as a prefix of those used at T_ℓ . Equivalently, if $\theta_t^{(m)} \stackrel{\text{iid}}{\sim} \pi$, then

$$(10) \quad T_\ell Y^{(m)}(x; T_\ell) = T_{\ell-1} Y^{(m)}(x; T_{\ell-1}) + \sum_{t=T_{\ell-1}+1}^{T_\ell} \mathcal{D}(x; \theta_t^{(m)}), \quad m = 1, \dots, M_\ell, \quad \ell = 1, \dots, L.$$

We define the coupled level increments by

$$(11) \quad \Delta Y^{(m)}(x; T_\ell) := Y^{(m)}(x; T_\ell) - Y^{(m)}(x; T_{\ell-1}), \quad m = 1, \dots, M_\ell, \quad \ell = 1, \dots, L.$$

The coupling ensures that $Y^{(m)}(x; T_\ell)$ and $Y^{(m)}(x; T_{\ell-1})$ are strongly correlated, so that $\Delta Y^{(m)}(x; T_\ell)$ typically has much smaller variance than either term alone. In particular, the telescoping identity holds [Gol08],

$$(12) \quad \mathbb{E}[Y^{(m)}(x; T_L)] = \mathbb{E}[Y^{(m)}(x; T_0)] + \sum_{\ell=1}^L \mathbb{E}[\Delta Y^{(m)}(x; T_\ell)] \quad m = 1, \dots, M_L.$$

2.5.2. *MLMC mean estimator and its variance estimator.* Motivated by (12), we define the MLMC estimator of $\mu(x)$ by

$$(13) \quad \mathcal{Y}(x; \mathbf{M}, \mathbf{T}) := \bar{Y}(x; M_0, T_0) + \sum_{\ell=1}^L \bar{\Delta Y}(x; M_\ell, T_\ell), \quad \bar{\Delta Y}(x; M_\ell, T_\ell) := \frac{1}{M_\ell} \sum_{m=1}^{M_\ell} \Delta Y^{(m)}(x; T_\ell).$$

where for each ℓ the samples $\{\Delta Y^{(m)}(x; T_\ell)\}_{m=1}^{M_\ell}$ are i.i.d. across m . We quantify the sampling variance of (13) using the empirical variance estimator

$$(14) \quad S_Y^2(x; \mathbf{M}, \mathbf{T}) := \frac{1}{M_0} \mathcal{S}_Y^2(x; M_0, T_0) + \sum_{\ell=1}^L \frac{1}{M_\ell} \mathcal{S}_{\Delta Y}^2(x; M_\ell, T_\ell),$$

where $\mathcal{S}_Y^2(x; M_0, T_0)$ is defined in (8) and

$$(15) \quad \mathcal{S}_{\Delta Y}^2(x; M_\ell, T_\ell) := \frac{1}{M_\ell - 1} \sum_{m=1}^{M_\ell} (\Delta Y^{(m)}(x; T_\ell) - \bar{\Delta Y}(x; T_\ell))^2,$$

2.5.3. *Moment identities.* The MLMC estimator (13) is unbiased for $\mu(x)$, and the expected value of the empirical variance estimator (14) is given by the variance μ_2 multiplied by function depending on \mathbf{T} and \mathbf{M} , respectively.

Lemma 2.6 (Moments of the MLMC mean estimator). *Let $\mathbf{T} = (T_0, \dots, T_L)$ satisfy (9) and suppose that, for each level ℓ , the outer samples $\{\Delta Y^{(m)}(x; T_\ell)\}_{m=1}^{M_\ell}$ are i.i.d. Then*

$$(16) \quad \mathbb{E}[\mathcal{Y}(x; \mathbf{M}, \mathbf{T})] = \mu(x),$$

and

$$(17) \quad \mathbb{E}[S_Y^2(x; \mathbf{M}, \mathbf{T})] = \mu_2(x) \left(\frac{1}{M_0 T_0} + \sum_{\ell=1}^L \frac{1}{M_\ell} \left(\frac{1}{T_{\ell-1}} - \frac{1}{T_\ell} \right) \right).$$

2.7. Multilevel estimator for the predictive variance. We next develop an MLMC estimator for the dropout-induced predictive variance $\mu_2(x)$. As in the single-fidelity setting, we estimate $\mu_2(x)$ using the unbiased sample variance $V(x, T)$ based on T stochastic forward passes. The multilevel construction mirrors that for the mean, but requires a careful coupling of variance estimators across fidelities.

2.7.1. Coupling via an online variance update. Fix $2 \leq T_0 < T_1 < \dots < T_L$ and let $\{\theta_t\}_{t=1}^{T_L}$ be i.i.d. draws from π . Assume in addition that $T_\ell - T_{\ell-1} \geq 2$ for $\ell = 1, \dots, L$, so that the unbiased sample variance on each new block is well-defined. For notational convenience write

$$D_t(x) := \mathcal{D}(x; \theta_t), \quad t = 1, \dots, T_L,$$

and define, for integers $1 \leq a < b$,

$$\bar{D}_{a:b}(x) := \frac{1}{b-a+1} \sum_{t=a}^b D_t(x), \quad V_{a:b}(x) := \frac{1}{b-a} \sum_{t=a}^b (D_t(x) - \bar{D}_{a:b}(x))^2.$$

With this notation the single-fidelity variance estimator in (6) is $V(x, T) = V_{1:T}(x)$.

To couple $V(x, T_{\ell-1})$ and $V(x, T_\ell)$, we reuse the first $T_{\ell-1}$ dropout draws in the T_ℓ -sample estimate and add only $T_\ell - T_{\ell-1}$ fresh draws. The resulting coupled variances satisfy the pooled-variance identity (equivalently, an online variance update) [CGL79]:

$$(18) \quad \begin{aligned} (T_\ell - 1)V(x, T_\ell) &= (T_{\ell-1} - 1)V(x, T_{\ell-1}) + (T_\ell - T_{\ell-1} - 1)V_{T_{\ell-1}+1:T_\ell}(x) \\ &+ \frac{T_{\ell-1}(T_\ell - T_{\ell-1})}{T_\ell} \left(\bar{D}_{1:T_{\ell-1}}(x) - \bar{D}_{T_{\ell-1}+1:T_\ell}(x) \right)^2. \end{aligned}$$

We define the coupled level increments by

$$(19) \quad \Delta V(x; T_\ell) := V(x; T_\ell) - V(x; T_{\ell-1}), \quad \ell = 1, \dots, L.$$

Since both $V(x; T_{\ell-1})$ and $V(x; T_\ell)$ are unbiased for $\mu_2(x)$ (Lemma 2.3), we have $\mathbb{E}[\Delta V(x; T_\ell)] = 0$, and the MLMC construction again relies on the reduced variance of the coupled differences.

2.7.2. MLMC variance estimator and its variance estimator. Let $\mathbf{T} = (T_0, \dots, T_L)$ and $\mathbf{M} = (M_0, \dots, M_L)$. For each level ℓ , we generate M_ℓ i.i.d. outer replicates of the coupled increment $\Delta V(x; T_\ell)$, and define the MLMC estimator of $\mu_2(x)$ by

$$(20) \quad \mathcal{V}(x; \mathbf{M}, \mathbf{T}) := \bar{V}(x; M_0, T_0) + \sum_{\ell=1}^L \bar{\Delta V}(x; M_\ell, T_\ell), \quad \bar{\Delta V}(x; M_\ell, T_\ell) := \frac{1}{M_\ell} \sum_{m=1}^{M_\ell} \Delta V^{(m)}(x; T_\ell).$$

We quantify the sampling variance of (20) using the empirical variance estimator

$$(21) \quad S_V^2(x; \mathbf{M}, \mathbf{T}) := \frac{1}{M_0} \mathcal{S}_V^2(x; M_0, T_0) + \sum_{\ell=1}^L \frac{1}{M_\ell} \mathcal{S}_{\Delta V}^2(x; M_\ell, T_\ell),$$

where $\mathcal{S}_V^2(x; M_0, T_0)$ is defined in (8) and

$$(22) \quad \mathcal{S}_{\Delta V}^2(x; M_\ell, T_\ell) := \frac{1}{M_\ell - 1} \sum_{m=1}^{M_\ell} (\Delta V^{(m)}(x; T_\ell) - \bar{\Delta V}(x; M_\ell, T_\ell))^2.$$

2.7.3. *Moment identities.* The MLMC estimator (20) is unbiased for $\mu_2(x)$, and the expected value of the empirical variance estimator (21) is solely dependent on the 2nd and 4th-order moments, \mathbf{M} , and \mathbf{T} .

Lemma 2.8 (Covariance of unbiased sample-variance estimators with overlapping samples). *Fix x and let $\{\theta_i\}_{i=1}^{T_\ell}$ be i.i.d. draws from π . Assume $\mathcal{D}(x; \theta)$ has finite fourth central moment and write $\mu_2(x)$ and $\mu_4(x)$ for the second and fourth central moments defined in (4) and (5). For $\ell \geq 1$, form $V(x; T_{\ell-1})$ from the first $T_{\ell-1}$ samples and $V(x; T_\ell)$ from the first T_ℓ samples. Then*

$$(23) \quad \text{Cov}[V(x; T_\ell), V(x; T_{\ell-1})] = \frac{T_{\ell-1} - 1}{T_\ell - 1} \text{Var}[V(x; T_{\ell-1})] + \frac{T_\ell - T_{\ell-1}}{T_{\ell-1} T_\ell (T_\ell - 1)} (\mu_4(x) - 3\mu_2^2(x)).$$

Theorem 2.9 (Moments of the MLMC variance estimator). *Let $\mathbf{T} = (T_0, \dots, T_L)$ with $T_0 \geq 2$ and suppose that, for each level ℓ , the outer samples $\{\Delta V^{(m)}(x; T_\ell)\}_{m=1}^{M_\ell}$ are i.i.d. Then*

$$(24) \quad \mathbb{E}[\mathcal{V}(x; \mathbf{M}, \mathbf{T})] = \mu_2(x),$$

and

$$(25) \quad \begin{aligned} \mathbb{E}[S_V^2(x; \mathbf{M}, \mathbf{T})] &= \frac{1}{M_0 T_0} \left(\mu_4(x) - \frac{T_0 - 3}{T_0 - 1} \mu_2^2(x) \right) + \sum_{\ell=1}^L \frac{1}{M_\ell} \left(\frac{1}{T_{\ell-1}} - \frac{1}{T_\ell} \right) (\mu_4(x) - 3\mu_2^2(x)) \\ &\quad + \sum_{\ell=1}^L \frac{2}{M_\ell} \left(\frac{1}{T_{\ell-1} - 1} - \frac{1}{T_\ell - 1} \right) \mu_2^2(x), \end{aligned}$$

where $\mu_4(x)$ is defined in (5).

Proof. The unbiasedness (24) follows from linearity of expectation and Lemma 2.3: $\mathbb{E}[V(x; T_0)] = \mu_2(x)$ and $\mathbb{E}[\Delta V(x; T_\ell)] = 0$. For the sampling variance, we have by the linearity of expectation that

$$(26) \quad \mathbb{E}[S_V^2(x; \mathbf{M}, \mathbf{T})] = \frac{1}{M_0} \mathbb{E}[S_V^2(x; M_0, T_0)] + \sum_{\ell=1}^L \frac{1}{M_\ell} \mathbb{E}[S_{\Delta V}^2(x; M_\ell, T_\ell)],$$

The definitions of S_V^2 and $S_{\Delta V}^2$ are that they are the unbiased variance estimators of V and ΔV respectively. Under the assumption that the outer samples are i.i.d., we have that expectation of the unbiased variance estimator is the variance, $\mathbb{E}[S_Z^2] = \text{Var}[Z]$, and thus

$$(27) \quad \mathbb{E}[S_V^2(x; \mathbf{M}, \mathbf{T})] = \frac{1}{M_0} \text{Var}[V(x; T_0)] + \sum_{\ell=1}^L \frac{1}{M_\ell} \text{Var}[\Delta V(x; T_\ell)].$$

Expanding the summand, we have the following expression

$$\text{Var}[\Delta V(x; T_\ell)] = \text{Var}[V(x; T_{\ell-1})] - 2\text{Cov}[V(x; T_{\ell-1}), V(x; T_\ell)] + \text{Var}[V(x; T_\ell)].$$

The first and last terms are given by Lemma 2.3. For $\ell \geq 1$, the coupling reuses the first $T_{\ell-1}$ stochastic forward passes inside the T_ℓ -sample variance. Hence, applying Lemma 2.8 to the nested pair $(V(x; T_{\ell-1}), V(x; T_\ell))$ gives a closed-form expression,

$$\text{Var}[\Delta V(x; T_\ell)] = \left(\frac{1}{T_{\ell-1}} - \frac{1}{T_\ell} \right) (\mu_4(x) - 3\mu_2^2(x)) + 2 \left(\frac{1}{T_{\ell-1} - 1} - \frac{1}{T_\ell - 1} \right) \mu_2^2(x),$$

which, upon substitution into the variance decomposition above, gives (25). \square

Remark 2.10. *The right-hand side of (25) is non-negative since it equals $\text{Var}[\mathcal{V}(x; \mathbf{M}, \mathbf{T})]$ by construction. Moreover, under the assumption of zero excess kurtosis, $\mu_4(x) = 3\mu_2^2(x)$, the expression (25) reduces to*

$$(28) \quad \mathbb{E}[S_V^2(x; \mathbf{M}, \mathbf{T})] = 2\mu_2^2(x) \left(\frac{1}{M_0} \frac{1}{T_0 - 1} + \sum_{\ell=1}^L \frac{1}{M_\ell} \left(\frac{1}{T_{\ell-1} - 1} - \frac{1}{T_\ell - 1} \right) \right).$$

In particular, for a geometric ladder (for example $T_\ell = 2^\ell T_0$) the single-level correction variances decay like $O(T_{\ell-1}^{-2})$, and the optimal allocation \mathbf{M} depends only on \mathbf{T} because the dependence on the underlying distribution enters through the common factor $2\mu_2^2(x)$.

3. COMPUTATION AND ALLOCATION

In this section we translate the estimators of Section 2 into a practical coupled sampling routine and then discuss how to allocate samples across fidelity levels to minimise sampling variance for a given computational budget.

3.1. Coupled sampling algorithm. The multilevel estimators for the predictive mean and variance rely on *coupled* evaluations within each level increment. For level $\ell \geq 1$ we compute $Y(x; T_{\ell-1})$ and $Y(x; T_\ell)$ (and similarly $V(x; T_{\ell-1})$ and $V(x; T_\ell)$) from the same underlying dropout realisations, reusing the first $T_{\ell-1}$ stochastic forward passes inside the T_ℓ -sample estimators. Algorithm 1 implements this coupling and returns the MLMC estimators $\mathcal{Y}(x; \mathbf{M}, \mathbf{T})$ and $\mathcal{V}(x; \mathbf{M}, \mathbf{T})$, along with the empirical variance estimators $S_Y^2(x; \mathbf{M}, \mathbf{T})$ and $S_V^2(x; \mathbf{M}, \mathbf{T})$ defined in (13)–(21).

Algorithm 1 Coupled sampling for MLMC mean and variance estimators

Require: input x ; fidelity ladder $\mathbf{T} = (T_0, \dots, T_L)$ with $2 \leq T_0 < \dots < T_L$; sample counts $\mathbf{M} = (M_0, \dots, M_L)$ with $M_\ell \geq 1$ and $M_\ell \geq 2$ whenever a sample variance is formed

Ensure: samples $\{Y^{(m)}(x; T_0), V^{(m)}(x; T_0)\}$ and increments $\{\Delta Y^{(m)}(x; T_\ell), \Delta V^{(m)}(x; T_\ell)\}$; estimators \mathcal{Y}, \mathcal{V} and empirical variances S_Y^2, S_V^2

- 1: Initialise arrays $\mathbf{Y}_0 \leftarrow [], \mathbf{V}_0 \leftarrow []$
- 2: **for** $m = 1$ to M_0 **do**
- 3: Draw T_0 i.i.d. $\theta^{(m)} \sim \pi$ and store evaluations $\mathbf{D}^{(m)} = [D_1^{(m)}, \dots, D_{T_0}^{(m)}]$ with $D_t^{(m)} = \mathcal{D}(x; \theta_t^{(m)})$
- 4: Compute $Y^{(m)} \leftarrow \text{mean}(\mathbf{D}^{(m)})$
- 5: Compute $V^{(m)} \leftarrow \text{sample_var}(\mathbf{D}^{(m)})$
- 6: Append $Y^{(m)}$ to \mathbf{Y}_0 and append $V^{(m)}$ to \mathbf{V}_0
- 7: **end for**
- 8: Initialise arrays $\mathbf{dY}_\ell \leftarrow [], \mathbf{dV}_\ell \leftarrow []$ for $\ell = 1, \dots, L$
- 9: **for** $\ell = 1$ to L **do**
- 10: **for** $m = 1$ to M_ℓ **do**
- 11: Draw $T_\ell - T_{\ell-1}$ i.i.d. $\theta^{(m)} \sim \pi$ and append evaluations $[D_{T_{\ell-1}+1}^{(m)}, \dots, D_{T_\ell}^{(m)}]$ to $\mathbf{D}^{(m)}$
- 12: Compute $Y_c^{(m)} \leftarrow \text{mean}([D_1^{(m)}, \dots, D_{T_{\ell-1}}^{(m)}])$ and $Y_f^{(m)} \leftarrow \text{mean}([D_1^{(m)}, \dots, D_{T_\ell}^{(m)}])$
- 13: Compute $V_c^{(m)} \leftarrow \text{sample_var}([D_1^{(m)}, \dots, D_{T_{\ell-1}}^{(m)}])$ and $V_f^{(m)} \leftarrow \text{sample_var}([D_1^{(m)}, \dots, D_{T_\ell}^{(m)}])$
- 14: Append $Y_f^{(m)} - Y_c^{(m)}$ to \mathbf{dY}_ℓ
- 15: Append $V_f^{(m)} - V_c^{(m)}$ to \mathbf{dV}_ℓ
- 16: **end for**
- 17: **end for**
- 18: Compute $\mathcal{Y} \leftarrow \text{mean}(\mathbf{Y}_0) + \sum_{\ell=1}^L \text{mean}(\mathbf{dY}_\ell)$
- 19: Compute $\mathcal{V} \leftarrow \text{mean}(\mathbf{V}_0) + \sum_{\ell=1}^L \text{mean}(\mathbf{dV}_\ell)$
- 20: Compute $S_Y^2 \leftarrow \text{sample_var}(\mathbf{Y}_0)/M_0 + \sum_{\ell=1}^L \text{sample_var}(\mathbf{dY}_\ell)/M_\ell$
- 21: Compute $S_V^2 \leftarrow \text{sample_var}(\mathbf{V}_0)/M_0 + \sum_{\ell=1}^L \text{sample_var}(\mathbf{dV}_\ell)/M_\ell$

3.2. Cost model. To compare single-fidelity and multilevel strategies we require a cost model. Throughout we measure cost by the number of stochastic forward passes of the trained network, that is, by the total number of calls to $\mathcal{D}(x; \theta)$ with independently drawn $\theta \sim \pi$. This proxy is appropriate when the dominant expense is the network evaluation itself and when overhead (such as reductions for computing means and variances) is negligible in comparison.

3.2.1. Uncoupled cost baseline. A useful baseline is the cost incurred if coarse and fine estimators were generated independently when forming each increment. In that uncoupled setting, level 0 requires $M_0 T_0$ evaluations, while for each $\ell \geq 1$ one would generate T_ℓ evaluations for the fine estimator, giving $M_\ell T_\ell$

evaluations at level ℓ . Hence the total uncoupled cost is

$$(29) \quad c_{\text{unc}} := M_0 T_0 + \sum_{\ell=1}^L M_\ell T_\ell,$$

3.2.2. *Effective cost under mask reuse.* In the common regime $M_0 \geq \dots \geq M_L$, a coupled single ℓ -level estimator draws T_ℓ dropout realisations and reuses the first $T_{\ell-1}$ of them to compute the coarse estimator. Therefore a coupled level- ℓ replicate costs $T_\ell - T_{\ell-1}$ evaluations rather than T_ℓ . The effective coupled cost is

$$(30) \quad c_{\text{cpl}} = T_0 M_0 + \sum_{\ell=1}^L (T_\ell - T_{\ell-1}) M_\ell = \sum_{\ell=0}^{L-1} T_\ell (M_\ell - M_{\ell+1}) + T_L M_L.$$

So that $c_{\text{cpl}} \leq c_{\text{unc}}$. For allocation we work with the coupled budget $c := c_{\text{cpl}}$.

3.3. **Optimal allocation across levels.** The MLMC estimators in Section 2 depend on the choice of sample counts $\mathbf{M} = (M_0, \dots, M_L)$. In this subsection we pose and solve the allocation problem: for a fixed computational budget, choose \mathbf{M} to minimise the sampling variance of the target estimator. We work with the coupled cost $c := c_{\text{cpl}}$ in the form (30). The optimisation is carried out over continuous M_ℓ and then rounded to integers in implementation.

3.3.1. *Allocation for the mean estimator.* The expectation of the empirical sampling variance of the MLMC mean estimator is given explicitly by Lemma 2.6. Writing

$$(31) \quad v_0(x) := \text{Var}[Y(x; T_0)] = \frac{\mu_2(x)}{T_0}, \quad v_\ell(x) := \text{Var}[\Delta Y(x; T_\ell)] = \mu_2(x) \left(\frac{1}{T_{\ell-1}} - \frac{1}{T_\ell} \right), \quad \ell \geq 1,$$

we have that the expectation of the empirical sampling variance of the expectation estimator is given by

$$(32) \quad \mathbb{E}[S_Y^2(x; \mathbf{M}, \mathbf{T})] = \frac{v_0(x)}{M_0} + \sum_{\ell=1}^L \frac{v_\ell(x)}{M_\ell}.$$

Minimising (32) subject to the budget constraint $c = T_0 M_0 + \sum_{\ell=1}^L (T_\ell - T_{\ell-1}) M_\ell$ yields the allocation in Lemma 3.4.

Lemma 3.4 (Optimal allocation for the mean estimator). *Fix x and a strictly increasing fidelity ladder $2 \leq T_0 < \dots < T_L$. Let $a_0 := T_0$ and $a_\ell := T_\ell - T_{\ell-1}$ for $\ell \geq 1$, and let $c > 0$ be the coupled-cost budget $c = \sum_{\ell=0}^L a_\ell M_\ell$. Among continuous choices $M_\ell > 0$ satisfying this budget constraint, the sampling variance $\mathbb{E}[S_Y^2(x; \mathbf{M}, \mathbf{T})]$ is minimised by*

$$(33) \quad M_\ell^* = c \frac{\sqrt{v_\ell(x)/a_\ell}}{\sum_{k=0}^L \sqrt{v_k(x)a_k}}, \quad \ell = 0, \dots, L.$$

Equivalently, substituting the explicit v_ℓ and a_ℓ yields

$$(34) \quad M_0^* = \frac{c}{T_0} \left(1 + \sum_{\ell=1}^L \frac{T_\ell - T_{\ell-1}}{\sqrt{T_\ell T_{\ell-1}}} \right)^{-1}, \quad M_i^* = \frac{c}{\sqrt{T_i T_{i-1}}} \left(1 + \sum_{\ell=1}^L \frac{T_\ell - T_{\ell-1}}{\sqrt{T_\ell T_{\ell-1}}} \right)^{-1}, \quad i = 1, \dots, L.$$

3.4.2. *Allocation for the variance estimator.* The sampling variance of the MLMC variance estimator is given by Theorem 2.9. Writing

$$(35) \quad w_0(x) := \text{Var}[V(x; T_0)], \quad w_\ell(x) := \text{Var}[\Delta V(x; T_\ell)], \quad \ell \geq 1,$$

we may express the objective as

$$(36) \quad \mathbb{E}[S_V^2(x; \mathbf{M}, \mathbf{T})] = \frac{w_0(x)}{M_0} + \sum_{\ell=1}^L \frac{w_\ell(x)}{M_\ell},$$

under the same budget constraint. In general $w_\ell(x)$ depends on $\mu_2(x)$ and $\mu_4(x)$, so in practice one either estimates $\{w_\ell(x)\}$ from pilot runs or uses a moment closure such as $\mu_4(x) = 3\mu_2^2(x)$, equation (28). The corresponding optimal allocations is given in Lemma 3.5.

Lemma 3.5 (Optimal allocation for the variance estimator). *Fix x and a fidelity ladder $2 \leq T_0 < \dots < T_L$. Let $a_0 := T_0$ and $a_\ell := T_\ell - T_{\ell-1}$ for $\ell \geq 1$, and let $c > 0$ be the coupled-cost budget $c = \sum_{\ell=0}^L a_\ell M_\ell$. Among continuous choices $M_\ell > 0$ satisfying the budget constraint, the expectation of the empirical sampling variance of the variance estimator,*

$$(37) \quad \mathbb{E}[S_V^2(x; \mathbf{M}, \mathbf{T})] = \frac{w_0(x)}{M_0} + \sum_{\ell=1}^L \frac{w_\ell(x)}{M_\ell}$$

is minimised by

$$(38) \quad M_\ell^* = c \frac{\sqrt{w_\ell(x)/a_\ell}}{\sum_{k=0}^L \sqrt{w_k(x)a_k}}, \quad \ell = 0, \dots, L.$$

3.6. Choosing the fidelity ladder. The multilevel constructions require a strictly increasing sequence of fidelities $\mathbf{T} = (T_0, \dots, T_L)$. In our setting T_ℓ is the number of stochastic forward passes used inside the single-replicate estimators $Y(x, T_\ell)$ and $V(x, T_\ell)$, so the ladder controls the variance–cost tradeoff through the coupled increment variances in Lemmas 2.6 and Theorem 2.9. We discuss practical choices of \mathbf{T} that are consistent with the couplings in Sections 2.5.1 and 2.7.1.

A convenient default is a geometric ladder

$$(39) \quad T_\ell := \lceil T_0 r^\ell \rceil, \quad \ell = 0, \dots, L,$$

with a fixed ratio $r > 1$ and smallest fidelity T_0 . This choice keeps neighbouring fidelities well separated while limiting the number of levels. In the present work we estimate both the predictive mean and the predictive variance, so we require $T_0 \geq 2$ in order for the unbiased sample variance $V(x, T_0)$ to be well-defined. Moreover, the variance coupling (18) involves the sample variance of the new block $V_{T_{\ell-1}+1:T_\ell}(x)$, hence we also impose

$$(40) \quad T_\ell - T_{\ell-1} \geq 2, \quad \ell = 1, \dots, L,$$

so that each refinement step introduces at least two new dropout draws. A simple and robust special case is the dyadic ladder

$$(41) \quad T_0 = 2, \quad T_\ell = 2^{\ell+1} \quad (\ell = 0, \dots, L),$$

which satisfies (40) exactly.

Given T_0 and r , the final level L is selected to reach a desired maximum inner fidelity T_{\max} , for example the number of dropout passes one would use in a conventional MC-dropout baseline. Concretely, we take

$$(42) \quad L := \max\{\ell \in \mathbb{N}_0 : T_\ell \leq T_{\max}\},$$

so that $T_L \leq T_{\max} < T_{L+1}$. In applications T_{\max} is set by an available evaluation budget per input or by a target error level for the inner estimators $Y(x, T)$ and $V(x, T)$.

The choice of the ratio r is primarily a practical modelling choice. If r is too close to 1 then L becomes large, which increases bookkeeping and may lead to levels with very small M_ℓ after allocation (in particular, if one wishes to estimate the sampling variances via S_Y^2 and S_V^2 , one typically requires $M_\ell \geq 2$ to form a non-degenerate sample variance). If r is too large then refinements add many new samples at once and the ladder behaves more like a small number of coarse-to-fine jumps. In the numerical results below we therefore adopt either the dyadic ladder (41) or the geometric ladder (39) with a moderate ratio (for example, $r = 2$), which respects (40) and keeps L small.

Finally, the ladder may also be selected adaptively using pilot samples. A standard stopping criterion is to increase L until the empirical contribution of the finest correction is negligible compared to the current estimator variance, for example until both

$$(43) \quad \frac{S_{\Delta Y}^2(x; M_L, T_L)}{M_L} \ll S_Y^2(x; \mathbf{M}, \mathbf{T}), \quad \frac{S_{\Delta V}^2(x; M_L, T_L)}{M_L} \ll S_V^2(x; \mathbf{M}, \mathbf{T}),$$

so that further refinement would not materially reduce the sampling variability at the current budget. This criterion is consistent with the variance decompositions in Lemma 2.6 and Theorem 2.9, and it naturally couples the choice of L with the allocation procedure in Section 3.3.

4. NUMERICAL EXPERIMENTS

This section evaluates the proposed multilevel estimators on two benchmark PINNs–Uzawa problems. The aim is to (i) verify the sampling theory of Sections 2–3, (ii) quantify the variance–cost tradeoff of MLMC relative to single-fidelity MC-dropout, and (iii) test the allocation formulas in Section 3.3 against brute-force enumeration under fixed cost.

4.1. Experimental setup and common definitions. All numerical results in this section are produced by repeated test-time evaluation of a fixed, trained surrogate network with dropout kept active. A single *network evaluation* is one stochastic forward pass $x \mapsto \mathcal{D}(x; \theta)$ with an independently resampled realisation $\theta \sim \pi$ (Section 2.1). All reported estimators are computed pointwise in x , and any norms or regression fits are subsequently applied to these pointwise quantities. Unless stated otherwise, the same implementation is used for both single-fidelity Monte Carlo and multilevel Monte Carlo, with coupling implemented within each level increment as in Algorithm 1.

4.1.1. Estimators and norms reported. Fix an evaluation grid $\{x_i\}_{i=1}^{N_x} \subset (0, 1)$. For a chosen inner fidelity $T \geq 2$ and outer sample count $M \geq 1$, we compute the single-fidelity estimators

$$Y^{(m)}(x_i, T) = \frac{1}{T} \sum_{t=1}^T \mathcal{D}(x_i; \theta_t^{(m)}), \quad V^{(m)}(x_i, T) = \frac{1}{T-1} \sum_{t=1}^T (\mathcal{D}(x_i; \theta_t^{(m)}) - Y^{(m)}(x_i, T))^2,$$

with $\theta_t^{(m)} \stackrel{\text{iid}}{\sim} \pi$, and then form the outer averages

$$\bar{Y}(x_i; M, T) = \frac{1}{M} \sum_{m=1}^M Y^{(m)}(x_i, T), \quad \bar{V}(x_i; M, T) = \frac{1}{M} \sum_{m=1}^M V^{(m)}(x_i, T),$$

together with their empirical outer-variance estimators

$$(44) \quad \begin{aligned} S_Y^2(x_i; M, T) &= \frac{1}{M-1} \sum_{m=1}^M (Y^{(m)}(x_i, T) - \bar{Y}(x_i; M, T))^2, \\ S_V^2(x_i; M, T) &= \frac{1}{M-1} \sum_{m=1}^M (V^{(m)}(x_i, T) - \bar{V}(x_i; M, T))^2. \end{aligned}$$

For multilevel experiments we use a fidelity ladder $\mathbf{T} = (T_0, \dots, T_L)$ and sample counts $\mathbf{M} = (M_0, \dots, M_L)$, and compute the coupled MLMC estimators $\mathcal{Y}(x_i; \mathbf{M}, \mathbf{T})$ and $\mathcal{V}(x_i; \mathbf{M}, \mathbf{T})$ and the associated empirical variance estimators $S_Y^2(x_i; \mathbf{M}, \mathbf{T})$ and $S_V^2(x_i; \mathbf{M}, \mathbf{T})$ as defined in Section 2 and implemented in Algorithm 1.

When a scalar summary over x is required (for example in variance–fidelity plots or fixed-cost surfaces), we report the discrete L^1 -proxy

$$(45) \quad \|g\|_{L^1} \approx \sum_{i=1}^{N_x} |g(x_i)| \Delta x, \quad \Delta x := x_{i+1} - x_i,$$

with Δx constant for a uniform grid. For log–log rate plots, we fit a linear model to $\log \|g\|_{L^1}$ against $\log T$ by least squares and report the estimated slope together with its confidence interval as indicated in the corresponding figure captions.

4.1.2. Cost accounting. We measure computational cost by the total number of stochastic forward passes of the trained network, that is, by the total number of calls to $\mathcal{D}(x; \theta)$ with independently drawn $\theta \sim \pi$ (Section 3.2). For a single-fidelity experiment with parameters (M, T) the cost is MT evaluations per input point.

For multilevel experiments we distinguish an uncoupled baseline cost, in which the coarse and fine estimators in each increment are generated independently, denoted c_{unc} , from the effective coupled cost in which the first $T_{\ell-1}$ samples are reused inside the T_ℓ -sample estimator, denoted c_{cpl} .

In the fixed-cost allocation studies, we enumerate integer tuples \mathbf{M} satisfying the chosen cost constraint (and any additional feasibility conditions such as $M_\ell \geq 2$ when a sample variance at level ℓ is required) and then compare empirical minima of the resulting estimator-variance surfaces with the theoretical allocations

from Section 3.3. Unless explicitly stated otherwise, all ‘‘fixed cost’’ multilevel experiments hold for c_{cpl} , equation (30), fixed.

4.2. Forward-PINNs benchmark: boundary layer problem. We begin with a forward model problem for which an explicit reference solution is available. This allows us to (i) visualise MC-dropout confidence bands, (ii) verify the single-fidelity sampling rates from Section 2, and (iii) test the fixed-cost allocation predictions from Section 3.

4.2.1. Problem definition and reference solution. For a parameter $\epsilon > 0$, we consider the boundary-layer problem

$$(46) \quad u(x) - \epsilon^2 u''(x) = 1 \quad \text{for } x \in (0, 1), \quad u(0) = u(1) = 0.$$

The exact solution is

$$(47) \quad u(x) = 1 - \frac{e^{x/\epsilon} + e^{(1-x)/\epsilon}}{1 + e^{1/\epsilon}}.$$

4.2.2. Training and architecture. We train a surrogate network \mathcal{D} using a PINNs–Uzawa setup for the boundary-layer problem (46), with dropout active in L_d layers. At test time, the trained deterministic weights are held fixed and the only source of randomness is from $\theta \sim \pi$, so each evaluation $\mathcal{D}(x; \theta)$ corresponds to one stochastic forward pass as in Section 2.1. The training hyperparameters used in this experiment are summarised in Table 1.

N_{in}	N_{out}	N_{width}	L_d	L_h	p_{drop}	N_{SGD}	N_{Uz}	N_{repeats}	γ	ρ	η	ϵ
1	1	64	3	0	0.1	50,000	50	5	100	0.01	0.5	1.0

TABLE 1. Hyperparameters used to train the forward (boundary-layer) surrogate. A single stochastic forward pass corresponds to evaluating $\mathcal{D}(x; \theta)$ with a freshly drawn random variable $\theta \sim \pi$. The parameters N_{in} , N_{out} , N_{width} , L_d , L_h , and p_{drop} are defined in the network architecture described in Section 2.1. The parameters N_{SGD} , N_{Uz} , and N_{repeats} denote the total number of training epochs, the number of epochs per Uzawa update, and the number of repeats used to compute the PINNs term each epoch, respectively. The parameter γ weights the boundary-condition term in the loss functional, ρ is the Uzawa update parameter, and η is the optimizer learning rate.

4.2.3. Single-fidelity behaviour as inner fidelity increases. We first illustrate how the inner fidelity T affects the single-fidelity Monte Carlo estimators. For each x we compute $Y(x, T)$ and $V(x, T)$ from (6) with $M = 1$ outer replicate, and plot the mean estimator together with the pointwise bands $Y(x, T) \pm \sqrt{V(x, T)}$ and $Y(x, T) \pm 2\sqrt{V(x, T)}$. The results in Figure 3 show that increasing T reduces visible sampling noise and yields smoother uncertainty bands.

4.2.4. Empirical verification of sampling-variance rates. We next verify the predicted T^{-1} scaling of the sampling variances. For each T we generate $M_0 = 10$ independent outer replicates of the single-fidelity estimators and compute the empirical estimator variances $\mathcal{S}_Y^2(\cdot; M_0, T)$ and $\mathcal{S}_V^2(\cdot; M_0, T)$ from (8). We report their discrete L^1 norms over the evaluation grid as described in Section 4.1. Figure 4 shows approximate log–log slopes close to -1 , consistent with Lemma 2.3.

4.2.5. Sensitivity to dropout probability. Fixing $T_0 = 10^4$ and $M_0 = 10$, we study how the empirical estimator variances depend on the dropout probability p_{drop} . Figure 5 shows that the variance decreases towards zero as $p_{\text{drop}} \rightarrow 0$ (deterministic evaluation) and increases as $p_{\text{drop}} \rightarrow 1$. To parameterise the trend we fit the generalised logit model

$$(48) \quad \log \|\mathcal{S}^2\|_{L^1} \approx \alpha_1 + \alpha_2 \log p_{\text{drop}}^{\alpha_4} - \alpha_3 \log (1 - p_{\text{drop}}^{\alpha_4}),$$

and report fitted parameters and confidence intervals in Table 2. This experiment is included as a secondary diagnostic and is not used in the MLMC constructions, where fidelity is controlled by T .

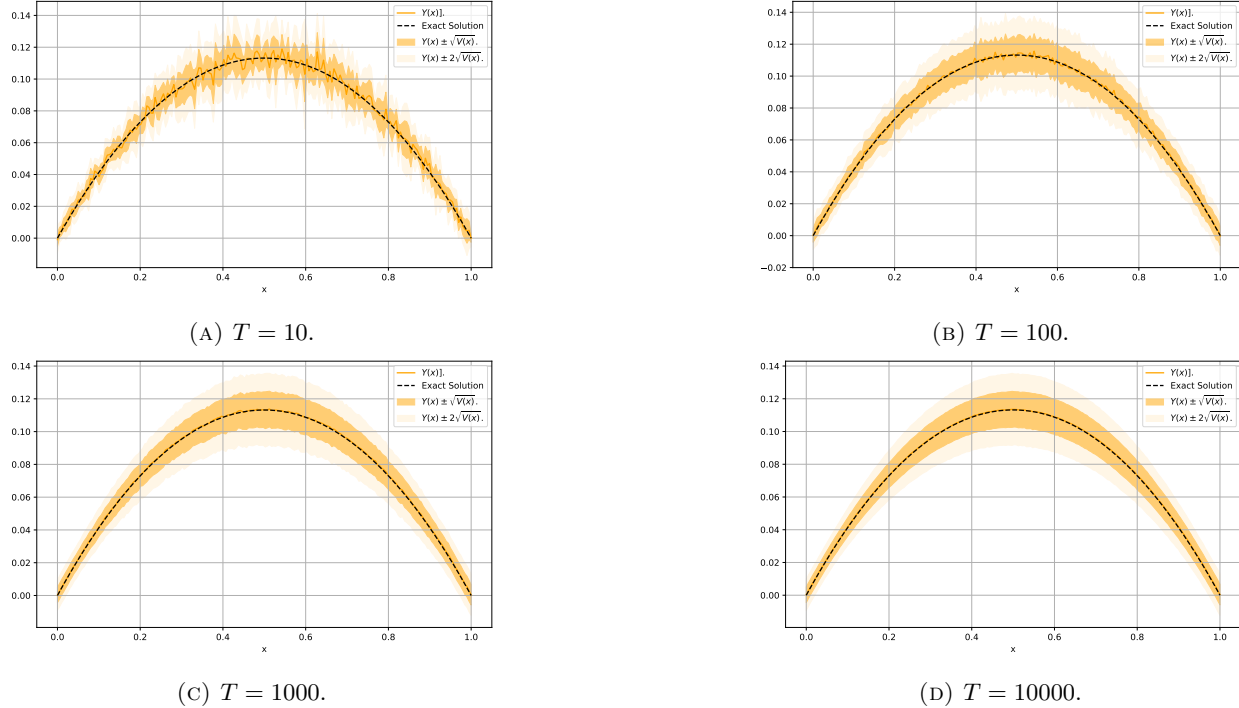


FIGURE 3. Single-fidelity single-level MC-dropout estimators at increasing inner fidelity T . Each subplot shows the estimated mean $Y(x, T)$ and the confidence bands $Y(x, T) \pm \sqrt{V(x, T)}$ and $Y(x, T) \pm 2\sqrt{V(x, T)}$. The exact solution (47) is shown as a dashed curve.

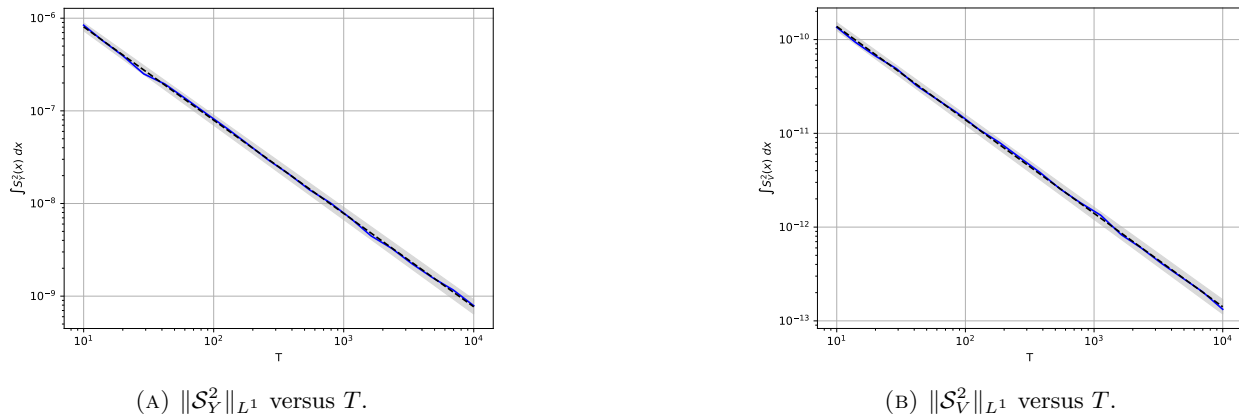


FIGURE 4. Empirical estimator variances versus inner fidelity T in the forward problem. Each subplot reports the discrete L^1 norm of the empirical outer-sample variance for the corresponding estimator, together with a log–log linear fit and a 99% confidence interval for the fitted slope.

	α_1	α_2	α_3	α_4
Y	-18.002 (-18.143, -17.862)	0.250 (0.223, 0.277)	3.259 (3.037, 3.481)	5.059 (4.373, 5.744)
V	-23.797 (-24.064, -23.531)	0.513 (0.476, 0.550)	8.307 (7.917, 8.697)	4.766 (4.306, 5.226)

TABLE 2. Fitted parameters for the model (48) in the forward problem. Parentheses denote 99% confidence intervals.

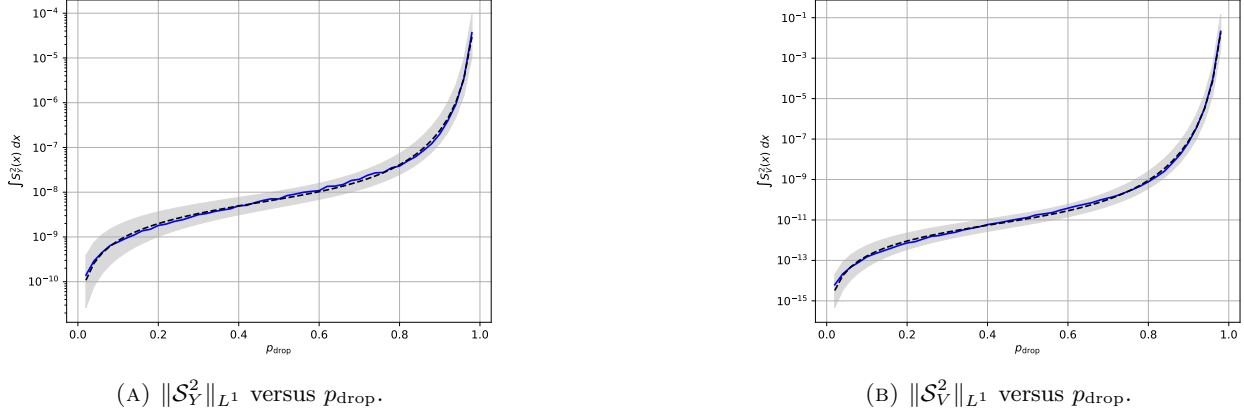


FIGURE 5. Dependence of empirical estimator variances on dropout probability p_{drop} for the forward problem at fixed $T_0 = 10^4$ and $M_0 = 10$. The dashed curves show the fitted model (48) with 99% confidence bands.

4.2.6. *Fixed-cost multilevel allocation test.* We now test the multilevel allocation theory under a fixed coupled-cost budget. We consider the three-level ladder

$$(49) \quad L = 2, \quad \mathbf{T} = (T_0, T_1, T_2) = (4, 8, 16), \quad c_{\text{cpl}} = 1000.$$

For each integer allocation $\mathbf{M} = (M_0, M_1, M_2)$ with $M_\ell \geq 2$ that satisfies the coupled-cost constraint (Subsubsection 4.1.2)

$$(50) \quad T_0 M_0 + (T_1 - T_0) M_1 + (T_2 - T_1) M_2 = c_{\text{cpl}},$$

we compute the empirical MLMC variance estimators $S_Y^2(\cdot; \mathbf{M}, \mathbf{T})$ and $S_V^2(\cdot; \mathbf{M}, \mathbf{T})$ from (14) and (21) using Algorithm 1. Since (50) leaves two degrees of freedom, we parameterise feasible allocations by (M_1, M_2) , with M_0 determined by the budget, and visualise the reciprocal surfaces $1/\|S_Y^2\|_{L^1}$ and $1/\|S_V^2\|_{L^1}$ to highlight minima. Figure 6 compares empirically best allocations with the continuous optimal allocations derived in Section 3.3, namely Lemma 3.4 for the mean estimator and Lemma 3.5 for the variance estimator (the latter under the zero-excess-kurtosis closure, equation (28), used in its derivation).

For the ladder $\mathbf{T} = (4, 8, 16)$ and cost $c_{\text{cpl}} = 1000$, the continuous optimal allocations predicted by the theory are independent of x for the mean estimator, and (under the zero-excess-kurtosis closure) independent of the underlying distribution up to an overall factor for the variance estimator. In particular, the mean-allocation formula yields $(M_0^*, M_1^*, M_2^*) = (1000/12, 1000/24, 1000/48)$, while the variance-allocation formula under the closure yields $(M_0^*, M_1^*, M_2^*) \approx (82.64, 44.17, 19.76)$.

4.3. **Inverse-PINNs benchmark: stochastic target source inference.** In this subsection we test the multilevel estimators on an inverse PINNs–Uzawa problem in which the training target is stochastic. This setting provides a closed-form reference for the target moments, and it lets us separate (i) Monte Carlo sampling error in estimating dropout-induced moments from (ii) surrogate mismatch due to imperfect training.

4.3.1. *Problem definition and ground-truth moments.* We consider the following constrained optimisation problem: given $\alpha > 0$ and a (possibly random) target $u_{\text{target}} \in L^2(0, 1)$, minimise

$$(51) \quad \frac{1}{2} \|u - u_{\text{target}}\|_{L^2(0,1)}^2 + \frac{\alpha}{2} \|f\|_{L^2(0,1)}^2$$

subject to the PDE constraint

$$(52) \quad -u''(x) = f(x) \quad \text{on } (0, 1), \quad u(0) = u(1) = f(0) = f(1) = 0.$$

For a synthetic benchmark with known moments, we generate stochasticity through a scalar noise variable

$$(53) \quad u_{\text{target}}(x) = (1 + \omega)(1 + \alpha\pi^4) \sin(\pi x), \quad \omega \sim \text{Unif}(-\delta/2, \delta/2),$$

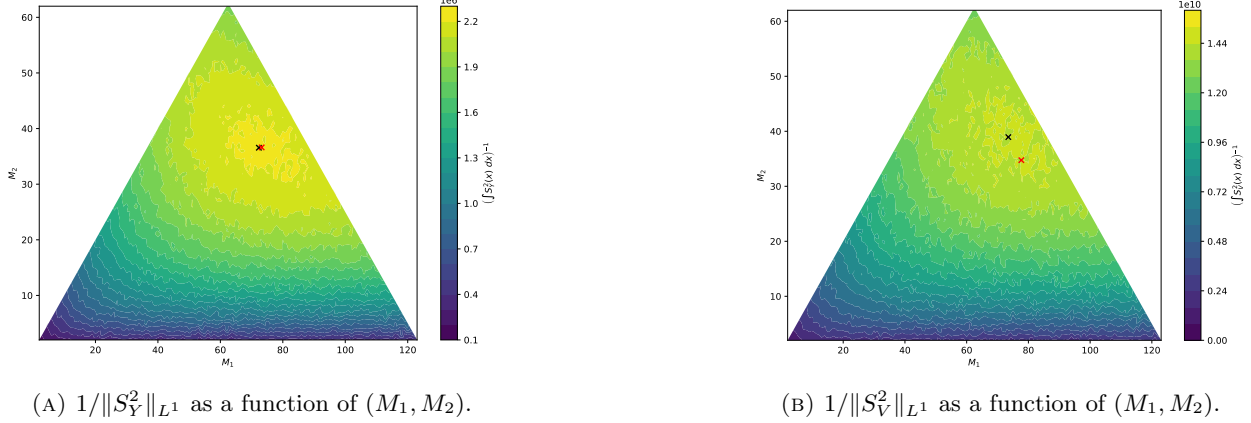


FIGURE 6. Fixed-cost allocation test for the forward problem with $\mathbf{T} = (4, 8, 16)$ and $c_{\text{cpl}} = 1000$. The black marker indicates an empirical minimiser over feasible integer allocations and the red marker indicates the continuous optimum from Lemma 3.4 (left) or Lemma 3.5 (right), noting that the variance-allocation formula is derived under the zero-excess-kurtosis closure.

and we use the closed-form family

$$(54) \quad u(x; \omega) = (1 + \omega) \sin(\pi x), \quad f(x; \omega) = (1 + \omega)\pi^2 \sin(\pi x).$$

The corresponding ground-truth moments are

$$(55) \quad \mathbb{E}[u(x)] = \sin(\pi x), \quad \mathbb{E}[f(x)] = \pi^2 \sin(\pi x),$$

and, using $\text{Var}(\omega) = \delta^2/12$,

$$(56) \quad \text{Var}[u(x)] = \frac{\delta^2}{12} \sin^2(\pi x), \quad \text{Var}[f(x)] = \frac{\delta^2}{12} \pi^4 \sin^2(\pi x).$$

These expressions provide a reference for assessing the empirical estimators of the dropout-induced moments computed as described in Subsection 4.1.

4.3.2. Surrogate model, architecture and hyperparameters. We train a two-output dropout network $\mathcal{D} = (\mathcal{U}, \mathcal{F})$ to approximate the solution pair (u, f) associated with (51)–(52) under the stochastic target (53). The architecture uses a shared trunk followed by branched heads for \mathcal{U} and \mathcal{F} , and we enforce the homogeneous Dirichlet boundary conditions by an output factor $x(1 - x)$. A schematic is shown in Figure 7, and the training hyperparameters are listed in Table 3.

At evaluation we hold the trained weights fixed and keep dropout active, so that each forward pass draws a fresh realisation $\theta \sim \pi$ and produces a stochastic prediction $\mathcal{D}(x; \theta)$. The estimators \mathcal{Y} , \mathcal{V} , S_Y^2 and S_V^2 are then computed from repeated stochastic forward passes exactly as described in Section 2 and implemented in Algorithm 1.

N_{in}	N_{out}	N_{width}	L_d	$L_{q,u}$	$L_{q,f}$	p_{drop}	N_{SGD}
1	2	128	4	0	1	0.2	200000
N_{Uz}	N_{repeats}	N_{lag}	α	β	η	ρ	δ
50	5	20	10^{-4}	10^{-4}	2.5×10^{-5}	10^{-3}	2.5×10^{-2}

TABLE 3. Hyperparameters used to train the inverse benchmark surrogate $\mathcal{D} = (\mathcal{U}, \mathcal{F})$. The architecture is the shared-trunk / branched-head dropout design and Figure 7. Many of the hyperparameters share the same definition as in Table 1. The hyperparameter β corresponds to the PINNs weight in the Loss functional, and N_{lag} is the number of evaluations per Uzawa update.

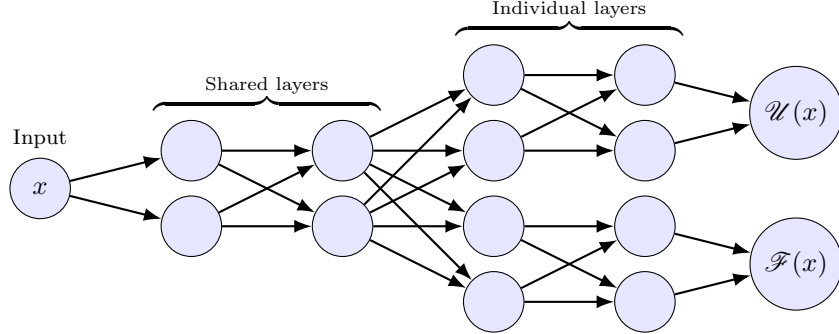


FIGURE 7. Schematic of the surrogate network architecture for the inverse benchmark. The network has a shared trunk of dropout layers followed by branched heads for \mathcal{U} and \mathcal{F} . A boundary-enforcing output factor $x(1 - x)$ is applied to each head.

4.3.3. *Single-fidelity behaviour: predictive means.* We first assess single-fidelity Monte Carlo estimation of the dropout-induced predictive means. For each output we compute $\bar{Y}(x; M, T)$ at a low inner fidelity $T = 10$ and a high inner fidelity $T = 10^4$ and compare to the ground-truth expectations (55). Figure 8 shows the estimated expectations and the corresponding pointwise errors.

4.3.4. *Single-fidelity behaviour: predictive variances.* We next assess single-fidelity estimation of the dropout-induced predictive variances via $V(x)$. We report standard deviations $\sqrt{V(x)}$ and compare to the analytical standard deviations obtained from (56). Results for $T = 10$ and $T = 10^4$ are shown in Figure 9.

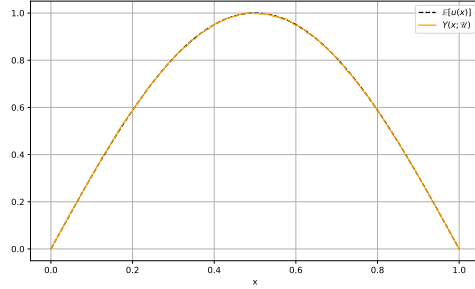
4.3.5. *Empirical verification of sampling-variance rates.* We now verify the predicted $\mathcal{O}(T^{-1})$ decay of the sampling variances of the single-fidelity estimators (Lemma 2.3). For each fidelity T we compute M_0 independent outer replicates and form the empirical outer-variance estimators $\mathcal{S}_Y^2(x; M_0, T)$ and $\mathcal{S}_V^2(x; M_0, T)$ for both outputs, then summarise their magnitudes using discrete L^1 norms over the evaluation grid as described in Subsubsection 4.1.1. Figure 10 reports the resulting log–log fits and Table 4 lists the estimated slopes and their 99% confidence intervals.

	lower 99% CI	est. gradient	upper 99% CI
$\mathcal{S}_Y^2(\mathcal{U})$	-1.0159	-1.0033	-0.9907
$\mathcal{S}_Y^2(\mathcal{F})$	-1.0094	-0.9976	-0.9857
$\mathcal{S}_V^2(\mathcal{U})$	-1.0000	-0.9852	-0.9704
$\mathcal{S}_V^2(\mathcal{F})$	-0.9963	-0.9842	-0.9722

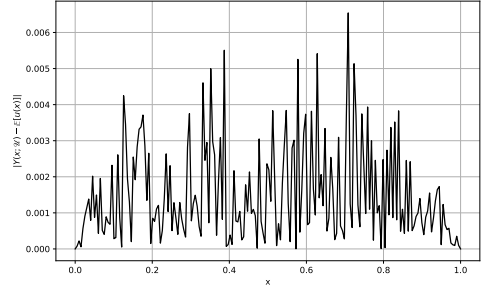
TABLE 4. Estimated log–log gradients of the single-fidelity sampling variances in Figure 10 with respect to T , together with 99% confidence intervals. We observe that the L^1 -norms of the estimator variances exhibit approximately $\mathcal{O}(T^{-1})$ decay.

4.3.6. *Fixed-cost multilevel allocation test.* We conclude with a fixed-cost allocation experiment for the multilevel estimators. We use a three-level ladder $\mathbf{T} = (T_0, T_1, T_2) = (4, 8, 16)$ (so $L = 2$) and a fixed coupled evaluation budget $c_{\text{cpl}} = 1000$ (subsubsection 4.1.2). We enumerate feasible integer allocations $\mathbf{M} = (M_0, M_1, M_2)$ satisfying $T_0 M_0 + (T_1 - T_0) M_1 + (T_2 - T_1) M_2 = c_{\text{cpl}}$ and the constraint $M_\ell \geq 2$. We enumerate feasible integer allocations $\mathbf{M} = (M_0, M_1, M_2)$ satisfying the budget and the constraint $M_\ell \geq 2$ (so that sample variances are defined), and we evaluate the empirical MLMC variance estimators \mathcal{S}_Y^2 and \mathcal{S}_V^2 for both outputs. For visualisation we plot reciprocal surfaces $1/\|\mathcal{S}^2\|_{L^1}$ as functions of (M_1, M_2) , noting that M_0 is then fixed by the cost constraint.

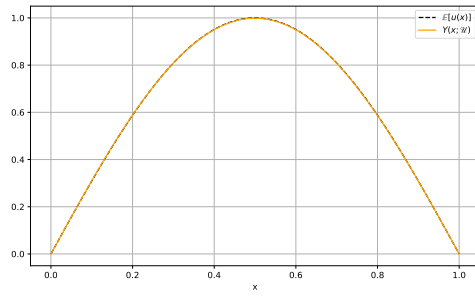
The black marker indicates an empirical minimiser over feasible integer allocations. The red marker indicates the continuous optimum obtained from the allocation formulas in § 3.3.1 for the mean estimator



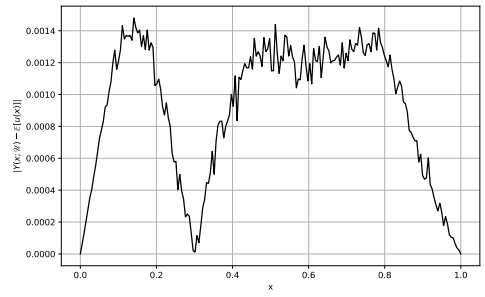
(A) $Y(\mathcal{U})$ vs. $\mathbb{E}[u]$, $T = 10$.



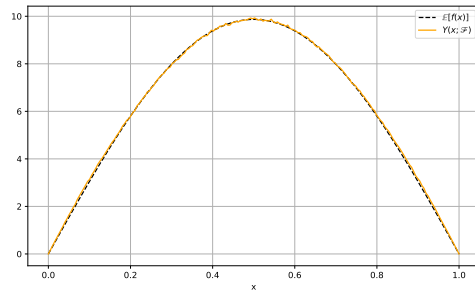
(B) Pointwise error for $Y(\mathcal{U})$, $T = 10$.



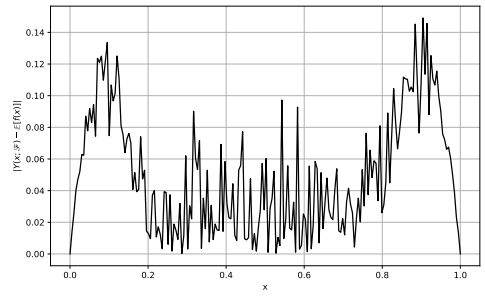
(C) $Y(\mathcal{U})$ vs. $\mathbb{E}[u]$, $T = 10^4$.



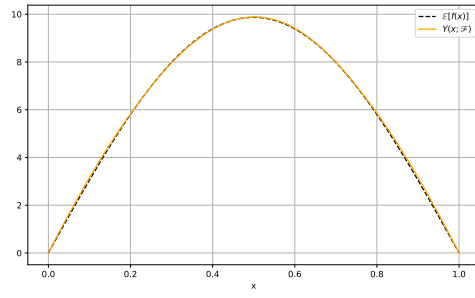
(D) Pointwise error for $Y(\mathcal{U})$, $T = 10^4$.



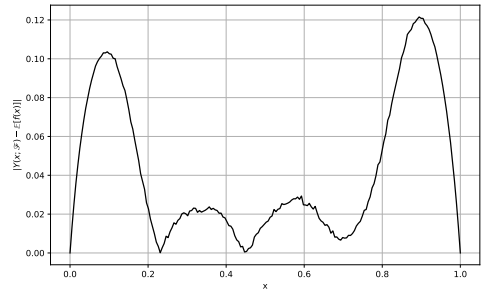
(E) $Y(\mathcal{F})$ vs. $\mathbb{E}[f]$, $T = 10$.



(F) Pointwise error for $Y(\mathcal{F})$, $T = 10$.



(G) $Y(\mathcal{F})$ vs. $\mathbb{E}[f]$, $T = 10^4$.



(H) Pointwise error for $Y(\mathcal{F})$, $T = 10^4$.

FIGURE 8. Single-fidelity single-level Monte Carlo estimation of predictive means for the inverse benchmark. The top two rows report $Y(x)$ for \mathcal{U} and compares it to $\mathbb{E}[u(x)]$ from (55); the bottom two rows report $Y(x)$ for \mathcal{F} and compares it to $\mathbb{E}[f(x)]$. For each output we show a low-fidelity estimate ($T = 10$) and a high-fidelity estimate ($T = 10^4$), together with the corresponding pointwise errors. In contrast to the variance estimates in Figure 9, the predictive means converge to the analytical expectations as T increases, indicating that the epistemic error is negligible compared to the Monte Carlo noise.

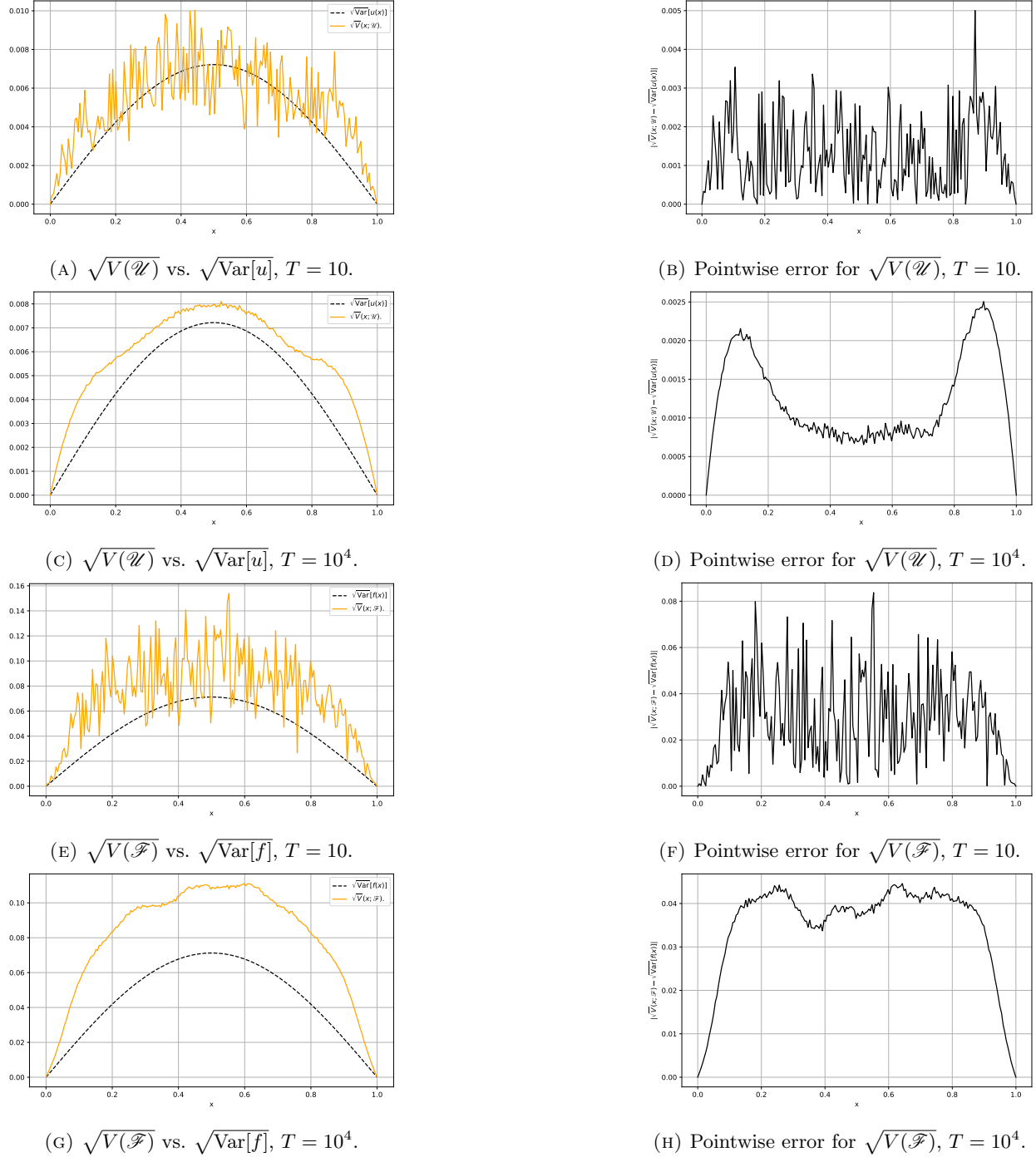


FIGURE 9. Single-fidelity single-level Monte Carlo estimation of predictive standard deviations for the inverse benchmark. The top row reports $\sqrt{V(x)}$ for \mathcal{U} and compares it to $\sqrt{\text{Var}[u(x)]}$ from (56); the bottom row reports $\sqrt{V(x)}$ for \mathcal{F} and compares it to $\sqrt{\text{Var}[f(x)]}$. Low- and high-fidelity results ($T = 10$ and $T = 10^4$) are shown together with pointwise errors. We observe that increasing T reduces the sampling noise in the estimator of V , the remaining discrepancy at high T reflects surrogate-induced epistemic mismatch rather than Monte Carlo error, indicating that the dropout posterior does not fully capture the aleatoric variability of the target mappings.

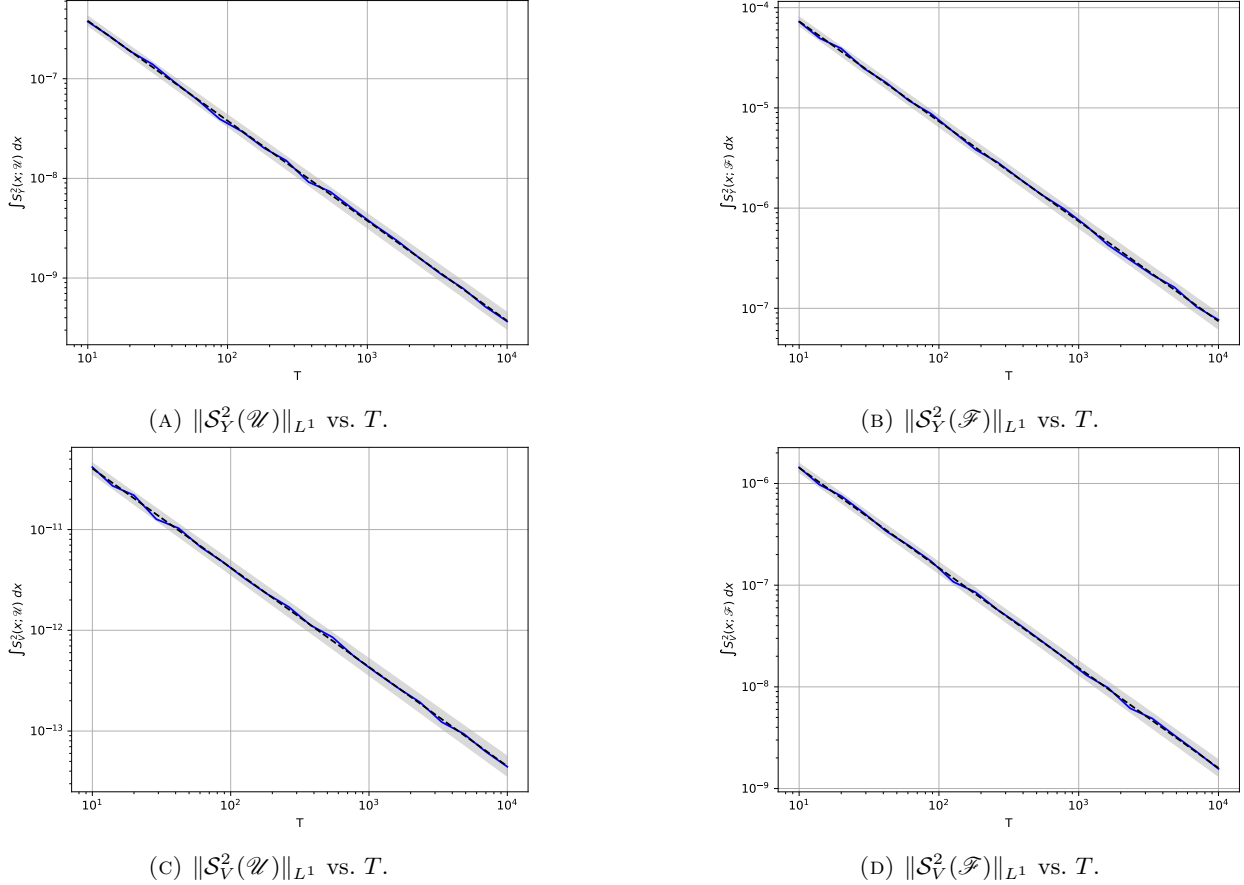


FIGURE 10. Empirical sampling-variance decay for the inverse benchmark. Each panel reports the discrete L^1 norm over the evaluation grid of the empirical sampling variance of a single-fidelity estimator as a function of the inner fidelity T . The dashed line is a linear fit on log–log axes and the shaded region indicates the 99% confidence interval for the fitted slope. The corresponding gradients are listed in Table 4.

and § 3.4.2 for the variance estimator (in the latter case under the zero-excess-kurtosis closure used for the simplified allocation).

The theoretical continuous optima for $\mathbf{T} = (4, 8, 16)$ and $c_{\text{cpl}} = 1000$ are the same as the previous problem, as the optimal \mathbf{M} depends solely on the fidelity ladder \mathbf{T} ,

$$(57) \quad \mathbf{M}_Y^* = \left(\frac{1000}{12}, \frac{1000}{24}, \frac{1000}{48} \right), \quad \mathbf{M}_V^* \approx (82.64, 44.17, 19.76),$$

where \mathbf{M}_Y^* is the mean-estimator allocation and \mathbf{M}_V^* is the variance-estimator allocation under the zero-excess-kurtosis closure.

5. CODE DISCUSSION

5.1. Reproducibility. All experiments are reproducible up to (i) the inherent stochasticity of dropout-based inference and (ii) non-determinism arising from GPU arithmetic and library implementations. In our code, pseudo-random number generators are seeded at the start of training using values specified in `CONFIG.py`, and the same seeding mechanism is available for evaluation to make figures repeatable when desired. Each training run creates a timestamped output directory in which the exact configuration file is copied and the trained model weights are saved, so that runs can be reloaded without ambiguity. While

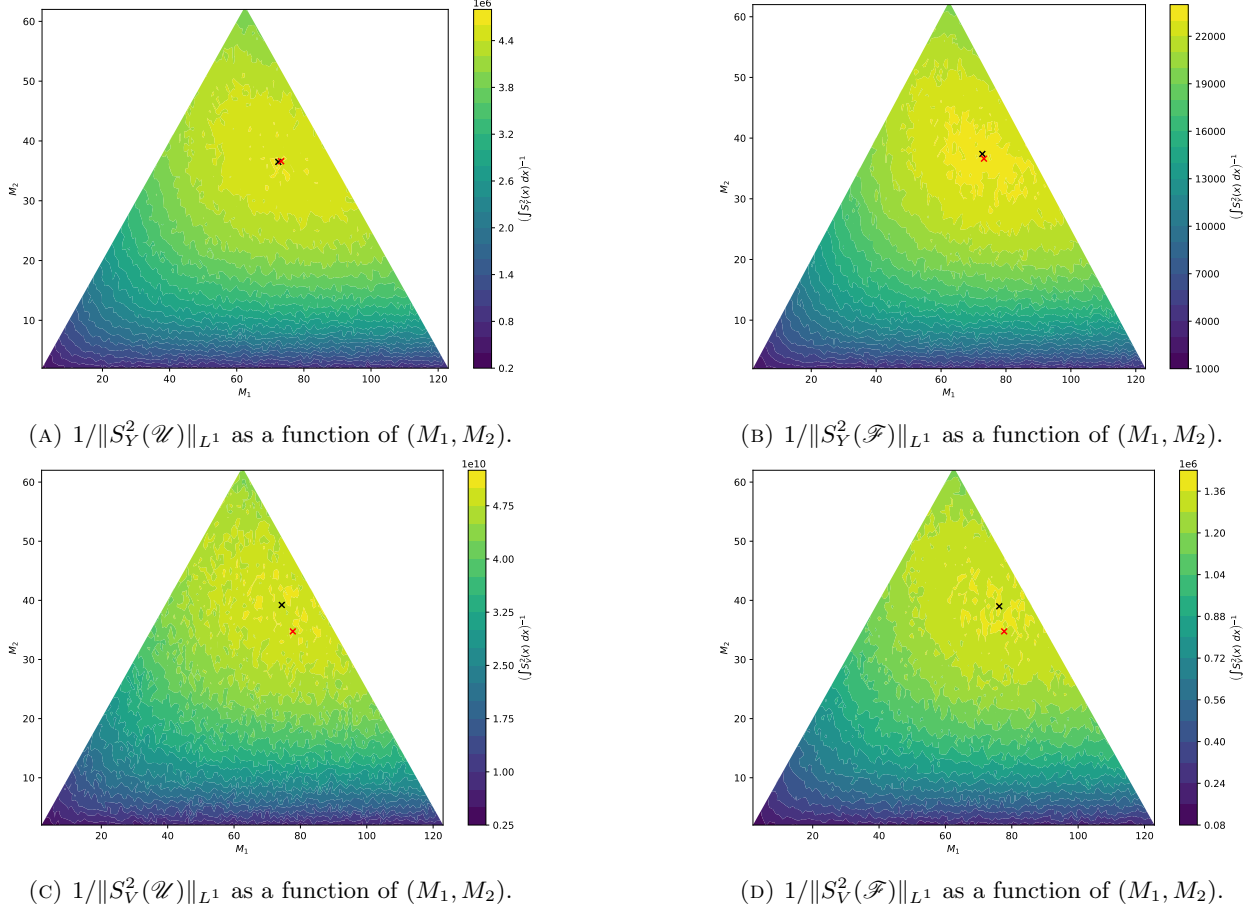


FIGURE 11. Fixed-cost allocation test for the inverse benchmark with $\mathbf{T} = (4, 8, 16)$ and $c_{\text{cppl}} = 1000$. Each panel shows the reciprocal variance surface of an MLMC estimator as a function of the integer allocations (M_1, M_2) , with M_0 determined by the coupled cost constraint. The black marker indicates an empirical minimiser over feasible integer allocations and the red marker indicates the continuous optimum given by the allocation formulas in § 3.3.1 (top row) and § 3.4.2 (bottom row, using the zero-excess-kurtosis closure for the simplified allocation).

these steps make results repeatable on the same software stack and hardware, bit-for-bit determinism is not guaranteed across different GPU architectures or different PyTorch/CUDA versions.

The code repository for this paper is available at https://github.com/aaronpim/Multilevel_Monte_Carlo_Dropout_PINNs.git.

5.2. Computational cost and implementation notes. Throughout, the operative notion of computational cost is the number of stochastic forward passes of the trained network, consistent with the cost models in Subsection 3.2. In particular, the coupled sampling strategy reuses dropout masks across fidelities and therefore reduces the number of additional network evaluations required to form multilevel increments compared with an uncoupled baseline.

In practice, the additional arithmetic required to aggregate samples into $Y(x, T)$, $V(x, T)$, and the multilevel estimators is negligible compared with the network evaluation cost for the architectures considered here. For this reason we do not attempt a hardware-specific FLOP accounting and instead report budgets and allocations in terms of forward-pass counts.

6. CONCLUSIONS

We have developed a multilevel Monte Carlo framework for MC-dropout in which epistemic uncertainty is induced by sampling dropout masks and fidelity is controlled by the number of stochastic forward passes. Coupling coarse and fine inner estimators through mask reuse, the resulting multilevel estimators for predictive means and variances remain unbiased for the corresponding dropout-induced quantities while substantially reducing sampling variance at a given evaluation budget. We derived explicit variance–cost relations, effective coupled cost models and principled sample allocation rules, and we verified these predictions on forward and inverse PINNs–Uzawa benchmarks, where the empirical variance rates and fixed-cost allocation experiments align with the theory up to the expected effects of integer feasibility and moment-closure assumptions.

APPENDIX A. SUPPLEMENTARY DERIVATIONS

A.1. Proofs of expectation and variance identities.

Proof of Lemma 2.3. The identities for $\mathbb{E}[Y]$ and $\text{Var}[Y]$ are standard. The unbiasedness of the sample variance implies $\mathbb{E}[V] = \mu_2$, and the expression for $\text{Var}[V]$ is a classical formula for the sampling variance of the unbiased variance estimator, stated for example in [Ben18, equation 10]. \square

Proof of Lemma 2.6. By linearity of expectation and (12),

$$\mathbb{E}[\mathcal{Y}(x; \mathbf{M}, \mathbf{T})] = \mathbb{E}[Y(x; T_0)] + \sum_{\ell=1}^L \mathbb{E}[\Delta Y(x; T_\ell)] = \mathbb{E}[Y(x; T_L)] = \mu(x),$$

where we used Lemma 2.3. Consider the the expectation of the empirical sampling variance of the expectation estimator, the linearity of expectation implies that

$$(58) \quad \mathbb{E}[S_Y^2(x; \mathbf{M}, \mathbf{T})] = \frac{1}{M_0} \mathbb{E}[\mathcal{S}_Y^2(x; M_0, T_0)] + \sum_{\ell=1}^L \frac{1}{M_\ell} \mathbb{E}[\mathcal{S}_{\Delta Y}^2(x; M_\ell, T_\ell)],$$

The definitions of \mathcal{S}_Y^2 and $\mathcal{S}_{\Delta Y}^2$ are that they are the unbiased variance estimators of Y and ΔY respectively. Under the assumption that the outer samples are i.i.d., we have that expectation of the unbiased variance estimator is the variance, $\mathbb{E}[\mathcal{S}_Z^2] = \text{Var}[Z]$, and therefore that

$$(59) \quad \mathbb{E}[S_Y^2(x; \mathbf{M}, \mathbf{T})] = \frac{1}{M_0} \text{Var}[Y(x; T_0)] + \sum_{\ell=1}^L \frac{1}{M_\ell} \text{Var}[\Delta Y(x; T_\ell)].$$

Under the coupling (10), $\Delta Y(x; T_\ell) = \frac{1}{T_\ell} \sum_{t=T_{\ell-1}+1}^{T_\ell} \mathcal{D}(x; \theta_t) - \frac{T_\ell - T_{\ell-1}}{T_\ell} Y(x; T_{\ell-1})$, and a direct computation using independence yields $\text{Var}[\Delta Y(x; T_\ell)] = \mu_2(x) \left(\frac{1}{T_{\ell-1}} - \frac{1}{T_\ell} \right)$, while Lemma 2.3 gives $\text{Var}[Y(x; T_0)] = \mu_2(x)/T_0$. \square

Proof of Lemma 2.8. Let D_1, \dots, D_{T_ℓ} be i.i.d, and let $\mu_k := \mathbb{E}[(X - \mu)^k]$ denote the k th central moment. Introduce the mean of the new block of size $T_\ell - T_{\ell-1}$,

$$(60) \quad \bar{D}_{T_{\ell-1}:T_\ell} := \frac{1}{T_\ell - T_{\ell-1}} \sum_{j=T_{\ell-1}+1}^{T_\ell} D_j.$$

A standard update identity due to [CGL79] states that

$$(61) \quad \begin{aligned} (T_\ell - 1)V(T_\ell) &= (T_{\ell-1} - 1)V(T_{\ell-1}) + \sum_{i=T_{\ell-1}+1}^{T_\ell} (D_i - \bar{D}_{T_{\ell-1}:T_\ell})^2 \\ &\quad + \frac{(T_\ell - T_{\ell-1})T_{\ell-1}}{T_\ell} (Y(T_{\ell-1}) - \bar{D}_{T_{\ell-1}:T_\ell})^2. \end{aligned}$$

The middle term on the right-hand side depends only on the new samples $D_{T_{\ell-1}+1}, \dots, D_{T_\ell}$ and is independent of $V(T_{\ell-1})$, hence its covariance with $V(T_{\ell-1})$ is zero. Taking covariance with $V(T_{\ell-1})$ in (61) and using bilinearity gives

$$(62) \quad \begin{aligned} (T_\ell - 1)\text{Cov}[V(T_\ell), V(T_{\ell-1})] &= (T_{\ell-1} - 1)\text{Var}[V(T_{\ell-1})] \\ &\quad + \frac{(T_\ell - T_{\ell-1})T_{\ell-1}}{T_\ell} \text{Cov}\left(\left(Y(T_{\ell-1}) - \bar{D}_{T_{\ell-1}:T_\ell}\right)^2, V(T_{\ell-1})\right). \end{aligned}$$

Since $\bar{D}_{T_{\ell-1}:T_\ell}$ is independent of $\{D_i\}_{i=1}^{T_{\ell-1}}$ and $\mathbb{E}[\bar{D}_{T_{\ell-1}:T_\ell}] = \mu$, a short expansion plus independence, and expressing the covariance as the product of their deviations yields

$$(63) \quad \text{Cov}\left(\left(Y(T_{\ell-1}) - \bar{D}_{T_{\ell-1}:T_\ell}\right)^2, V(T_{\ell-1})\right) = \mathbb{E}\left[\left(Y(T_{\ell-1}) - \mu\right)^2\left(V(T_{\ell-1}) - \mu_2\right)\right].$$

It remains to compute the expectation on the right-hand side. Write $\xi_i := D_i - \mu$, then $Y(T) - \mu = \frac{1}{T} \sum_{i=1}^T \xi_i$ and

$$(64) \quad (T_{\ell-1} - 1)V(T_{\ell-1}) = \sum_{i=1}^{T_{\ell-1}} \xi_i^2 - T_{\ell-1} \left(Y(T_{\ell-1}) - \mu\right)^2.$$

Using (64),

$$(65) \quad \mathbb{E}\left[\left(Y(T_{\ell-1}) - \mu\right)^2 V(T_{\ell-1})\right] = \frac{1}{T_{\ell-1} - 1} \mathbb{E}\left[\left(Y(T_{\ell-1}) - \mu\right)^2 \sum_{i=1}^{T_{\ell-1}} \xi_i^2\right] - \frac{T_{\ell-1}}{T_{\ell-1} - 1} \mathbb{E}\left[\left(Y(T_{\ell-1}) - \mu\right)^4\right].$$

A direct index-counting argument gives

$$(66) \quad \mathbb{E}\left[\left(Y(T_{\ell-1}) - \mu\right)^2 \sum_{i=1}^{T_{\ell-1}} \xi_i^2\right] = \frac{1}{T_{\ell-1}^2} \mathbb{E}\left[\left(\sum_{i=1}^{T_{\ell-1}} \xi_i\right)^2 \left(\sum_{k=1}^{T_{\ell-1}} \xi_k^2\right)\right] = \frac{\mu_4}{T_{\ell-1}} + \frac{T_{\ell-1} - 1}{T_{\ell-1}} \mu_2^2,$$

and similarly

$$(67) \quad \mathbb{E}\left[\left(Y(T_{\ell-1}) - \mu\right)^4\right] = \frac{\mu_4}{T_{\ell-1}^3} + \frac{3(T_{\ell-1} - 1)}{T_{\ell-1}^3} \mu_2^2.$$

Substituting (66)–(67) into (65) yields

$$(68) \quad \mathbb{E}\left[\left(Y(T_{\ell-1}) - \mu\right)^2 V(T_{\ell-1})\right] = \frac{\mu_4}{T_{\ell-1}^2} + \frac{T_{\ell-1} - 3}{T_{\ell-1}^2} \mu_2^2.$$

Since $\mathbb{E}\left[\left(Y(T_{\ell-1}) - \mu\right)^2\right] = \mu_2/T_{\ell-1}$, we obtain

$$(69) \quad \mathbb{E}\left[\left(Y(T_{\ell-1}) - \mu\right)^2 \left(V(T_{\ell-1}) - \mu_2\right)\right] = \left(\frac{\mu_4}{T_{\ell-1}^2} + \frac{T_{\ell-1} - 3}{T_{\ell-1}^2} \mu_2^2\right) - \frac{\mu_2}{T_{\ell-1}} \mu_2 = \frac{1}{T_{\ell-1}^2} (\mu_4 - 3\mu_2^2).$$

Combining (62), (63) and (69) gives

$$(T_\ell - 1)\text{Cov}[V(T_\ell), V(T_{\ell-1})] = (T_{\ell-1} - 1)\text{Var}[V(T_{\ell-1})] + \frac{T_\ell - T_{\ell-1}}{T_{\ell-1} T_\ell} (\mu_4 - 3\mu_2^2).$$

Dividing by $T_\ell - 1$ yields the first line of (23). The $\text{Var}[V(T_{\ell-1})]$ term may be directly evaluated using the closed form for $\text{Var}[V(T_{\ell-1})]$, which is $\frac{1}{T_{\ell-1}} (\mu_4 - \frac{T_{\ell-1} - 3}{T_{\ell-1} - 1} \mu_2^2)$. \square

A.2. Proofs of optimal allocation results.

Proof of Lemma 3.4. Fix x and $\mathbf{T} = (T_0, \dots, T_L)$ with $1 \leq T_0 < \dots < T_L$. Recall the additive coupled-cost representation

$$(70) \quad c = T_0 M_0 + \sum_{\ell=1}^L (T_\ell - T_{\ell-1}) M_\ell = \sum_{\ell=0}^L a_\ell M_\ell, \quad a_0 := T_0, \quad a_\ell := T_\ell - T_{\ell-1} \ (\ell \geq 1),$$

and the variance decomposition

$$(71) \quad \mathbb{E}[S_Y^2(x; \mathbf{M}, \mathbf{T})] = \frac{v_0(x)}{M_0} + \sum_{\ell=1}^L \frac{v_\ell(x)}{M_\ell},$$

where

$$(72) \quad v_0(x) = \frac{\mu_2(x)}{T_0}, \quad v_\ell(x) = \mu_2(x) \left(\frac{1}{T_{\ell-1}} - \frac{1}{T_\ell} \right) = \mu_2(x) \frac{T_\ell - T_{\ell-1}}{T_\ell T_{\ell-1}}, \quad \ell \geq 1.$$

On the open set $\{M_\ell > 0\}_{\ell=0}^L$, the objective $\sum_{\ell=0}^L v_\ell(x)/M_\ell$ is strictly convex and the constraint $\sum_{\ell=0}^L a_\ell M_\ell = c$ is affine, so any stationary point is the unique global minimiser.

Introduce the Lagrangian

$$(73) \quad \mathcal{L}(\mathbf{M}, \lambda) := \sum_{\ell=0}^L \frac{v_\ell(x)}{M_\ell} + \lambda \left(\sum_{\ell=0}^L a_\ell M_\ell - c \right).$$

The first-order optimality conditions are, for each ℓ ,

$$(74) \quad \frac{\partial \mathcal{L}}{\partial M_\ell} = -\frac{v_\ell(x)}{M_\ell^2} + \lambda a_\ell = 0, \quad \Rightarrow \quad M_\ell = \sqrt{\frac{v_\ell(x)}{\lambda a_\ell}}.$$

Using (72), we obtain

$$(75) \quad \frac{v_0(x)}{a_0} = \frac{\mu_2(x)}{T_0^2}, \quad \frac{v_\ell(x)}{a_\ell} = \frac{\mu_2(x)}{T_\ell T_{\ell-1}} \quad (\ell \geq 1),$$

hence (74) implies

$$(76) \quad M_0 = \frac{\sqrt{\mu_2(x)}}{\sqrt{\lambda}} \frac{1}{T_0}, \quad M_\ell = \frac{\sqrt{\mu_2(x)}}{\sqrt{\lambda}} \frac{1}{\sqrt{T_\ell T_{\ell-1}}}, \quad \ell = 1, \dots, L.$$

Enforcing the budget constraint (70) gives

$$(77) \quad \begin{aligned} c &= T_0 M_0 + \sum_{\ell=1}^L (T_\ell - T_{\ell-1}) M_\ell \\ &= \frac{\sqrt{\mu_2(x)}}{\sqrt{\lambda}} \left(1 + \sum_{\ell=1}^L \frac{T_\ell - T_{\ell-1}}{\sqrt{T_\ell T_{\ell-1}}} \right), \end{aligned}$$

so

$$(78) \quad \frac{\sqrt{\mu_2(x)}}{\sqrt{\lambda}} = c \left(1 + \sum_{\ell=1}^L \frac{T_\ell - T_{\ell-1}}{\sqrt{T_\ell T_{\ell-1}}} \right)^{-1}.$$

Substituting (78) into (76) yields (33). The factor $\mu_2(x)$ cancels, so the optimal allocation depends only on \mathbf{T} and c . \square

Proof of Lemma 3.5. We seek to minimise the expectation of the empirical sampling variance of the variance estimator

$$(79) \quad \mathbb{E}[S_V^2(x; \mathbf{M}, \mathbf{T})] = \frac{w_0(x)}{M_0} + \sum_{\ell=1}^L \frac{w_\ell(x)}{M_\ell}$$

subject to the same coupled-cost constraint

$$(80) \quad c = \sum_{\ell=0}^L a_\ell M_\ell, \quad a_0 := T_0, \quad a_\ell := T_\ell - T_{\ell-1} \quad (\ell \geq 1).$$

As in the proof of Lemma 3.4, strict convexity of $\sum w_\ell/M_\ell$ for $M_\ell > 0$ implies that the KKT stationary point is the unique global minimiser. Introducing the Lagrangian

$$\mathcal{L}(\mathbf{M}, \lambda) := \sum_{\ell=0}^L \frac{w_\ell(x)}{M_\ell} + \lambda \left(\sum_{\ell=0}^L a_\ell M_\ell - c \right),$$

the first-order conditions give

$$(81) \quad -\frac{w_\ell(x)}{(M_\ell^*)^2} + \lambda a_\ell = 0, \quad \Rightarrow \quad M_\ell^* = \sqrt{\frac{w_\ell(x)}{\lambda a_\ell}}.$$

Enforcing the budget constraint (80) gives

$$(82) \quad c = \sum_{k=0}^L \sqrt{\frac{w_k(x)a_k}{\lambda}}, \quad \sqrt{\lambda} = \frac{1}{c} \sum_{k=0}^L \sqrt{w_k(x)a_k}, \quad M_\ell^* = c \frac{\sqrt{w_\ell(x)/a_\ell}}{\sum_{k=0}^L \sqrt{w_k(x)a_k}}.$$

□

REFERENCES

- [Ben18] E. Benhamou. “A few properties of sample variance”. In: *arXiv preprint arXiv:1809.03774* (2018).
- [Bla+23] J. Blanchet et al. “Dropout training is distributionally robust optimal”. In: *Journal of Machine Learning Research* 24.180 (2023), pp. 1–60.
- [CGL79] T. F. Chan, G. H. Golub, and R. J. LeVeque. *Updating formulae and a pairwise algorithm for computing sample variances*. Tech. rep. STAN-CS-79-773. Stanford University, Department of Computer Science, Nov. 1979.
- [Cli+11] K. A. Cliffe et al. “Multilevel Monte Carlo methods and applications to elliptic PDEs with random coefficients”. In: *Computing and Visualization in Science* 14.1 (2011), p. 3.
- [Cox+24] A. M. Cox et al. “A Bayesian inverse approach to proton therapy dose delivery verification”. In: *Proceedings A*. Vol. 480. 2301. The Royal Society. 2024, p. 20230836.
- [FS21] M. Fujisawa and I. Sato. “Multilevel monte carlo variational inference”. In: *Journal of Machine Learning Research* 22.278 (2021), pp. 1–44.
- [Gal16] Y. Gal. “Uncertainty in deep learning”. PhD thesis. University of Cambridge, 2016.
- [Gaw+23] J. Gawlikowski et al. “A survey of uncertainty in deep neural networks”. In: *Artificial Intelligence Review* 56.Supp1 1 (2023), pp. 1513–1589.
- [Ger+21] T. Gerstner et al. “Multilevel Monte Carlo learning”. In: *arXiv preprint arXiv:2102.08734* (2021).
- [GG16] Y. Gal and Z. Ghahramani. “Dropout as a bayesian approximation: Representing model uncertainty in deep learning”. In: *international conference on machine learning*. PMLR. 2016, pp. 1050–1059.
- [Gil08] M. B. Giles. “Multilevel monte carlo path simulation”. In: *Operations research* 56.3 (2008), pp. 607–617.
- [Gil15] M. B. Giles. “Multilevel monte carlo methods”. In: *Acta numerica* 24 (2015), pp. 259–328.
- [Guo+17] C. Guo et al. “On calibration of modern neural networks”. In: *International conference on machine learning*. PMLR. 2017, pp. 1321–1330.
- [Hei01] S. Heinrich. “Multilevel monte carlo methods”. In: *International Conference on Large-Scale Scientific Computing*. Springer. 2001, pp. 58–67.
- [Hik+25] Y. Hikida et al. “Multilevel neural simulation-based inference”. In: *arXiv preprint arXiv:2506.06087* (2025).
- [HW21] E. Hüllermeier and W. Waegeman. “Aleatoric and epistemic uncertainty in machine learning: An introduction to concepts and methods”. In: *Machine learning* 110.3 (2021), pp. 457–506.
- [KG17] A. Kendall and Y. Gal. “What uncertainties do we need in bayesian deep learning for computer vision?” In: *Advances in neural information processing systems* 30 (2017).

- [LPB17] B. Lakshminarayanan, A. Pritzel, and C. Blundell. “Simple and scalable predictive uncertainty estimation using deep ensembles”. In: *Advances in neural information processing systems* 30 (2017).
- [MBK21] X. Meng, H. Babaee, and G. E. Karniadakis. “Multi-fidelity Bayesian neural networks: Algorithms and applications”. In: *Journal of Computational Physics* 438 (2021), p. 110361.
- [MPP24] C. G. Makridakis, A. Pim, and T. Pryer. “A Deep Uzawa-Lagrange Multiplier Approach for Boundary Conditions in PINNs and Deep Ritz Methods”. In: *arXiv preprint arXiv:2411.08702* (2024).
- [PP25] A. Pim and T. Pryer. “Surrogate Modelling of Proton Dose with Monte Carlo Dropout Uncertainty Quantification”. In: *arXiv preprint arXiv:2509.18155* (2025).
- [RPK19] M. Raissi, P. Perdikaris, and G. E. Karniadakis. “Physics-informed neural networks: A deep learning framework for solving forward and inverse problems involving nonlinear partial differential equations”. In: *Journal of Computational physics* 378 (2019), pp. 686–707.
- [Sri+14] N. Srivastava et al. “Dropout: a simple way to prevent neural networks from overfitting”. In: *The journal of machine learning research* 15.1 (2014), pp. 1929–1958.
- [YMK21] L. Yang, X. Meng, and G. E. Karniadakis. “B-PINNs: Bayesian physics-informed neural networks for forward and inverse PDE problems with noisy data”. In: *Journal of Computational Physics* 425 (2021), p. 109913.

¹ INSTITUTE FOR MATHEMATICAL INNOVATION, UNIVERSITY OF BATH, BATH, UK. ² DEPARTMENT OF MATHEMATICAL SCIENCES, UNIVERSITY OF BATH, BATH, UK.